The Astrophysical Journal, 774:101 (22pp), 2013 September 10 doi:10.1088/0004-637X/774/2/101

THE GALEX NEARBY YOUNG-STAR SURVEY

David R. Rodriguez[1], B. Zuckerman[2], Joel H. Kastner[3], M. S. Bessell[4],
Jacqueline K. Faherty[1,5], and Simon J. Murphy[4,6]
[1] Departamento de Astronomía, Universidad de Chile, Casilla 36-D, Santiago, Chile; drodrigu@das.uchile.cl
[2] Department of Physics and Astronomy, University of California, Los Angeles, CA 90095, USA
[3] Center for Imaging Science and Laboratory for Multiwavelength Astrophysics,
Rochester Institute of Technology, 54 Lomb Memorial Drive, Rochester, NY 14623, USA
[4] The Australian National University, Cotter Road, Weston Creek, ACT 2611, Australia
[5] Department of Astrophysics, American Museum of Natural History, Central Park West at 79th Street, New York, NY 10034, USA
[6] Gliese Fellow, Astronomisches Rechen-Institut, Zentrum für Astronomie der Universität Heidelberg, D-69120 Heidelberg, Germany
Received 2013 March 22; accepted 2013 June 28; published 2013 August 21

ABSTRACT

We describe a method that exploits data from the *Galaxy Evolution Explorer* (*GALEX*) ultraviolet and *Wide-field Infrared Survey Explorer* and Two Micron All Sky Survey infrared source catalogs, combined with proper motions and empirical pre-main sequence isochrones, to identify candidate nearby, young, low-mass stars. Applying our method across the full *GALEX*-covered sky, we identify 2031 mostly M-type stars that, for an assumed age of 10 (100) Myr, all lie within ∼150 (∼90) pc of Earth. The distribution of M spectral subclasses among these ∼2000 candidate young stars peaks sharply in the range M3–M4; these subtypes constitute 50% of the sample, consistent with studies of the M star population in the immediate solar neighborhood. We focus on a subset of 58 of these candidate young M stars in the vicinity of the Tucana–Horologium association. Only 20 of these 58 candidates were detected in the ROSAT All-Sky X-ray Survey—reflecting the greater sensitivity of *GALEX* for the purposes of identifying active nearby, young stars, particularly for stars of type M4 and later. Based on statistical analysis of the kinematics and/or spectroscopic followup of these 58 M stars, we find that 50% (29 stars) indeed have properties consistent with Tuc–Hor membership, while 12 are potential new members of the Columba association, and 2 may be AB Dor moving group members. Hence, ∼75% of our initial subsample of 58 candidates are likely members of young (age ∼ 10–40 Myr) stellar moving groups within 100 pc, verifying that the stellar color- and kinematics-based selection algorithms described here can be used to efficiently isolate nearby, young, low-mass objects from among the field star population. Future studies will focus on characterizing additional subsamples selected from among this list of candidate nearby, young M stars.

Key words: open clusters and associations: individual (Tuc–Hor, Columba) – stars: evolution – stars: pre-main sequence – ultraviolet: stars

Online-only material: color figures

1. INTRODUCTION

The past two decades have seen the discovery of a number of young (age < 100 Myr) stellar moving groups and associations within ∼100 pc of Earth (for reviews, see Zuckerman & Song 2004; Torres et al. 2008). By studying stars in these moving groups, one can observe the evolution of stellar properties as a function of juvenile ages. Nearby young stars and brown dwarfs are excellent targets for studies of gas-rich circumstellar disks (e.g., Qi et al. 2004, 2006, 2008; Hughes et al. 2008; Kastner et al. 2008; Rodriguez et al. 2010; Zuckerman & Song 2012) and direct imaging surveys of young Jupiters (e.g., Chauvin et al. 2004, 2005; Marois et al. 2008, 2010; Lagrange et al. 2010). At present, the membership of these young stellar groups are poorly determined for spectral types later than ∼M2 (e.g., Torres et al. 2008; Shkolnik et al. 2011; Schlieder et al. 2012b). In contrast, the field population of M dwarfs peaks strongly at spectral types M3–M5 (see Farihi et al. 2005; Henry et al. 2006; Reid et al. 2007; Bochanski et al. 2010; Stelzer et al. 2013 and references therein) suggesting a significant number of nearby, young stars with spectral types later than M3 remains to be discovered. The identification of additional young moving group members, particularly low-mass stars, is a key step both in our understanding of the processes involved in the early stages of stellar and substellar evolution and in searches for recently formed planets.

Given the incompleteness of the young moving groups at the low-mass end, many programs are actively searching for these "missing" M-dwarfs with a variety of techniques (e.g., see Rodriguez et al. 2011; Riedel et al. 2011; Shkolnik et al. 2011, 2012; Schlieder et al. 2012b; Malo et al. 2013 and references therein). Several techniques exploit the ultraviolet (UV) and X-ray properties of low-mass stars. As low-mass ($M < 1\,M_{\odot}$) pre-main sequence stars descend to the main sequence, their deep convective envelopes combine with differential rotation to produce strong magnetic dynamos. This stellar dynamo generates high levels of chromospheric and coronal activity; the former is a source of UV emission while the latter contributes to X-ray emission (Linsky et al. 2001; Preibisch & Feigelson 2005; Stelzer et al. 2013). Recent work (Findeisen et al. 2011; Rodriguez et al. 2011; Shkolnik et al. 2011; Findeisen & Hillenbrand 2010) has linked stellar activity due to youth with UV emission detected with the *Galaxy Evolution Explorer* (*GALEX*) satellite (Martin et al. 2005). Shkolnik et al. (2011) suggest that such UV-bright low-mass stars have ages ∼ 300 Myr or younger, based on the strength of their X-ray emission (see Section 6 in Shkolnik et al. 2011). These low-mass stars are brightest at near-infrared (IR) wavelengths and

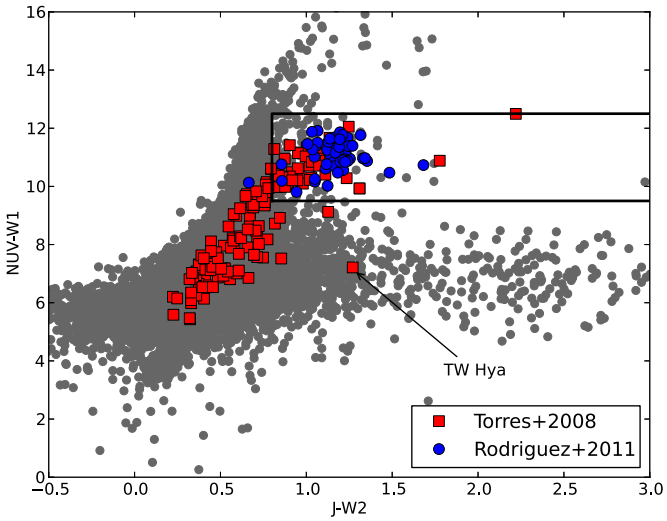

Figure 1. NUV–$W1$ vs. $J-W2$ magnitudes for field sources detected in *GALEX* and *WISE*/2MASS as well as members (or candidates) of nearby, young moving groups (Torres et al. 2008; Rodriguez et al. 2011). The ordinate is NUV–$W1$ color from *GALEX* and *WISE* ($W1$ corresponds to 3.4 μm emission) and the abscissa is $J-W2$ color from 2MASS and *WISE* ($W2$ corresponds to 4.6 μm emission). The rectangle shows our color selection criteria (see Table 1 and Section 2.1). Young stars with $J-W2 > 1$ are readily distinguished from older main sequence stars which have $J-W2 < 1$ and NUV–$W1$ between 10 and 14; $J-W2$ can be used a proxy for spectral type (see Equation (2) and Figure 4). Distant UV-bright galaxies are the diffuse cloud of objects with NUV–$W1$ between 5–9 and $J-W2 > 1$. TW Hya is the object located at $J-W2 \sim 1.3$ and NUV–$W1 \sim 7$; Rodriguez et al. (2011) suggest its unique location in UV–IR colors is due to the accretion within the system.

(A color version of this figure is available in the online journal.)

thus are best identified with surveys such as the Two Micron All Sky Survey (2MASS; Cutri et al. 2003). The recent release of the *Wide-field Infrared Survey Explorer* (*WISE*) catalog (Wright et al. 2010) has opened up the sky at additional near- to mid-IR wavelengths beyond those covered with 2MASS, facilitating the identification of cooler and fainter low-mass objects. The bright UV emission from the stellar chromosphere, combined with cool-star colors at optical and IR wavelengths, make the *GALEX* source catalog a powerful tool to search for nearby, young, low-mass stars.

Our prior work tying together UV emission with near-IR photometry was carried out for the Scorpius–Centaurus region and TW Hya association (TWA; Rodriguez et al. 2011). That study introduced a method to identify candidate young stars via the combination of their (1) UV–IR colors, (2) estimated range of motion in the context of Galactic space velocities for known young stellar groups, and (3) spectral signatures of youth. In the present work, we extend our methodology to incorporate the *WISE* data, which permits characterization of the full spectral energy distribution of UV-bright stars, allows estimation of proper motions (PMs, given the ~10 yr baseline between *WISE* and 2MASS), and breaks the *JHK*s color degeneracy for early- to mid-M dwarfs. We have also now extended our initial study to the entire *GALEX*-covered sky (61% of the total sky), allowing detection of thousands of candidate young low-mass stars, some of which may be members of previously undiscovered moving groups. We have also devised an algorithm to identify such potential stellar groups based on their similar PMs and estimated distances (Section 3.1) and have carried out a convergent point analysis for several young moving groups (Section 3.2). We refer to these collected efforts to identify young stars through the combination of *GALEX* and other catalog data as the *GALEX* Nearby Young-Star Survey (GALNYSS). Here, we describe our methodology and present the first GALNYSS results, with a focus on the Tucana–Horologium association.

Table 1
Selection Criteria Used for Our *GALEX*–*WISE*–2MASS Search

	Selection Criteria
(1)	$9.5 \leqslant \mathrm{NUV} - W1 < 12.5$
(2)	$J - W2 \geqslant 0.8$
(3)	$0 < W1 - W2 < 0.6$
(4)	n_2mass = 1
(5)	$W2 \geqslant 6$
(6)	$W2 \leqslant 14$
(7)	$W2 \leqslant 12$ for $1.7 < J - W2 < 3.3$

Notes. The first three expressions are used to select UV-bright dwarfs with spectral types late-K to early-L. The remaining criteria facilitate our search by filtering out crowded regions, saturated stars, and possible faint galaxies. In Criterion 4, n_2mass is a flag from the WISE catalog indicating the number of 2MASS sources within 3″ (see details in Section 2.1).

2. GALNYSS METHODOLOGY

We have developed a search strategy that consists of combining the *GALEX*, 2MASS, and *WISE* catalog information to identify nearby, young, low-mass stars. This is similar to the work presented in Rodriguez et al. (2011), but revised to utilize *WISE* data as well as improved isochrones and selection criteria. The steps in our identification sequence are as follows.

1. Combine IR and UV photometry to identify objects likely to be nearby, M-type dwarfs with UV excesses (Section 2.1).
2. Use cataloged and calculated PMs (Section 2.2), combined with estimates of spectral types and photometric distances (Section 2.3), to select the subset of these objects that are candidate M-type stars within ~150 pc (if 10 Myr old) and have *UVW* space motions similar to those of known young stellar groups (Section 2.4).
3. Perform spectroscopic follow up of the best resulting candidates (Section 2.5) to measure radial velocities along with spectral features, such as Hα emission and Li absorption lines, that are diagnostic of youth (Section 2.6).

2.1. *GALEX* (UV-based) Identification of Candidate Nearby, Young, Low-mass Stars

To identify candidate young, low-mass stars, we first examine where in various color–color combinations known young stars (as drawn from Rodriguez et al. 2011; Torres et al. 2008) lie with respect to other field *GALEX* sources. Figure 1 demonstrates this in a combined *GALEX*–*WISE*–2MASS NUV–$W1$ versus $J-W2$ color–color diagram. Here NUV is the near UV *GALEX* channel, $W1$ and $W2$ are the 3.4 and 4.6 μm *WISE* bands and J is from the 2MASS catalog. As we demonstrate in Section 2.3, $J-W2$ color can be used as a proxy for spectral type. In Figure 1, the young low-mass stars from Torres et al. (2008) and Rodriguez et al. (2011) stand out with respect to earlier-type young stars, older field stars, and the galaxy population. The $J-W2$ colors of young, low-mass stars are red and, while their NUV–$W1$ colors are bluer than those of field stars, they are not as blue as typical galaxies (NUV–$W1$ colors between 5 and 9).

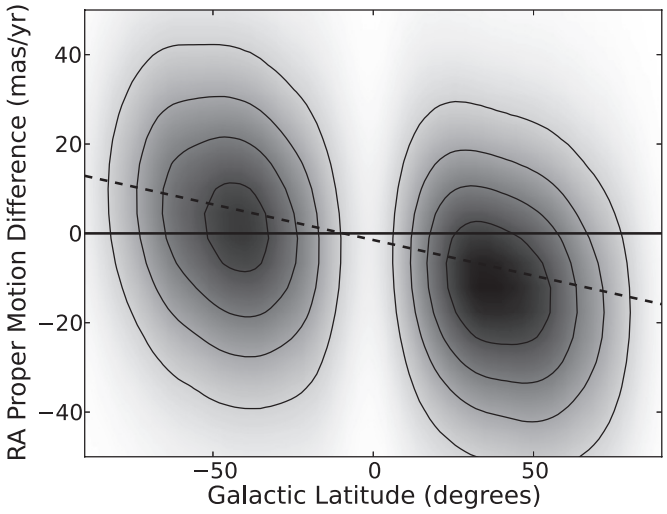

Figure 2. Density plot of R.A. proper motion differences for 300,000 sources. *WISE*–2MASS proper motions are compared to PPMXL as a function of galactic latitude. A similar trend is observed when comparing to UCAC4 or USNO-B1. As these were originally drawn from our *GALEX* tables, no coverage exists for galactic latitudes <10 deg. While a similar discrepancy can also be seen in ecliptic longitude, it is corrected most easily in Galactic coordinates. The dashed line indicates the correction used (Section 2.2).

Figure 1 drives our main selection criteria, which are listed in Table 1. The first two criteria define where known young, low-mass stars are located in color–color space. Criterion 3 is used to ensure our empirical spectral type relationship and isochrones are valid (see Section 2.3). Criterion 4 (a flag from the *WISE* catalog) ensures there is only one 2MASS source associated with a given *WISE* source within 3″. This avoids misassociation of IR sources in crowded fields, though such confusion is worst near the Galactic plane, where *GALEX* has not observed. The remaining criteria are used to avoid saturated sources and to exclude contaminating, background galaxies. We note that members of young moving groups listed in Torres et al. (2008) are removed from the GALNYSS candidate tables prior to our analysis, to avoid re-identifying known young stars. However, other lists of proposed young stars (e.g., Zuckerman & Song 2004; Rodriguez et al. 2011) are not excluded.

2.2. *WISE–2MASS Proper Motions*

We make use of PM information to distinguish between candidate young stars and other UV excess sources, such as background galaxies or nearby flare stars. We have cross-correlated our sample against the UCAC4 (Zacharias et al. 2012) and PPMXL (Roeser et al. 2010) PM catalogs. In total, ∼56% and ∼98% of our color-selected candidates have matches with objects listed in these respective catalogs. Comparison with other catalogs shows that 92% of the UV excess sources have PMs in SuperCosmos (Hambly et al. 2001) and 70% in USNO-B1 (Monet et al. 2003). For any source that lacked a published PM, a PM was estimated directly from the *WISE*–2MASS astrometry. With the ∼10 yr baseline and 3″ cross-correlation radius, these catalogs provide reasonable estimates of PM (up to ∼300 mas yr^{-1}) suitable for the first steps in our analysis. We note, however, a small (∼10–15 mas yr^{-1}) systematic offset in the *WISE*–2MASS PMs in the R.A. direction as a function of galactic latitude. Figure 2 shows this offset when examining over 300,000 sources in the PPMXL catalog. Similar results are found when comparing with UCAC4 and USNO-B1. The *WISE* Explanatory Supplement[7] mentions that, given that the *WISE* astrometry is tied to that of 2MASS and no PM information was considered for the 10 yr baseline, the *WISE* coordinate frame has a distortion relative to the International Celestial Reference System. A full correction is beyond the scope of this paper, but we attempt to remedy the R.A. offset with a linear term:

$$\mu_{\rm R.A.} = \mu_{\rm R.A._0} - 0.15963 \times b - 1.48284. \quad (1)$$

Here, $\mu_{\rm R.A._0}$ and $\mu_{\rm R.A.}$ are the PMs in the R.A. direction before and after the correction. We note that this offset is smaller than the uncertainty we describe below.

Figure 3 compares PMs estimated from *WISE*–2MASS astrometry to those from PPMXL for the final list of ∼2000 candidates in this study (see Section 2.5). From the rms scatter, we conservatively adopt 25 mas yr^{-1} as an estimate of the uncertainty for objects without PMs in published catalogs. We thus have at least one PM estimate for each candidate object, though in practice most objects have several estimates in good agreement with each other.

[7] See http://wise2.ipac.caltech.edu/docs/release/allsky/expsup/sec6_4.html.

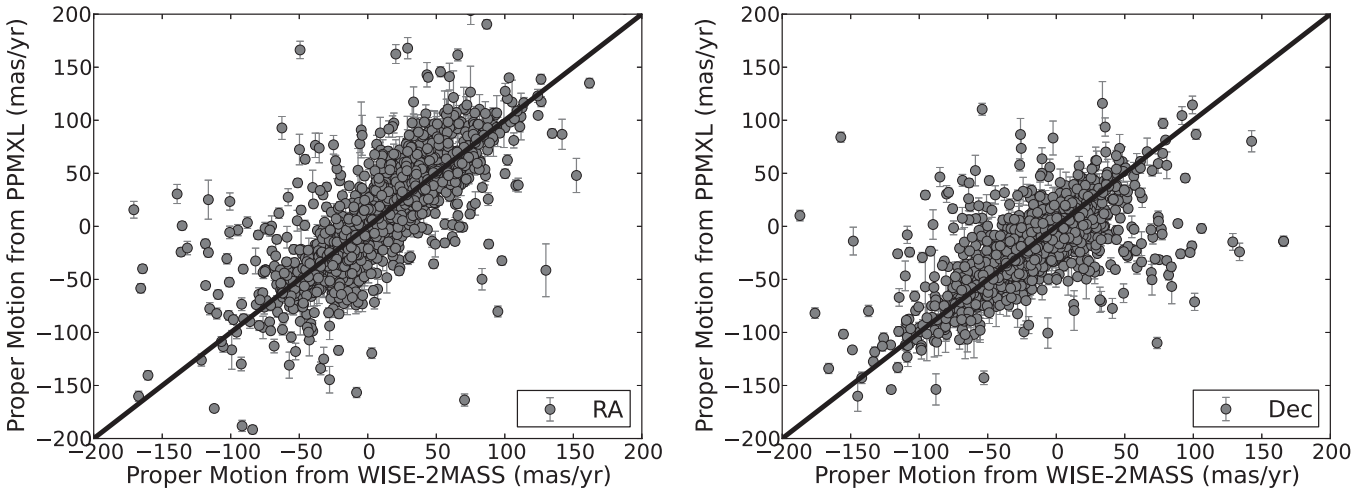

Figure 3. Proper motions from PPMXL compared to those we have derived from *WISE*–2MASS astrometry for the stars in this study. The rms scatter is ∼25 mas yr^{-1}. Similar results are found when comparing *WISE*–2MASS proper motions against those listed in the UCAC3, USNO-B1, SuperCosmos, or UCAC4 catalogs. A small (∼10–15 mas yr^{-1}) systematic offset in R.A. proper motion has been corrected (see Section 2.2 and Figure 2).

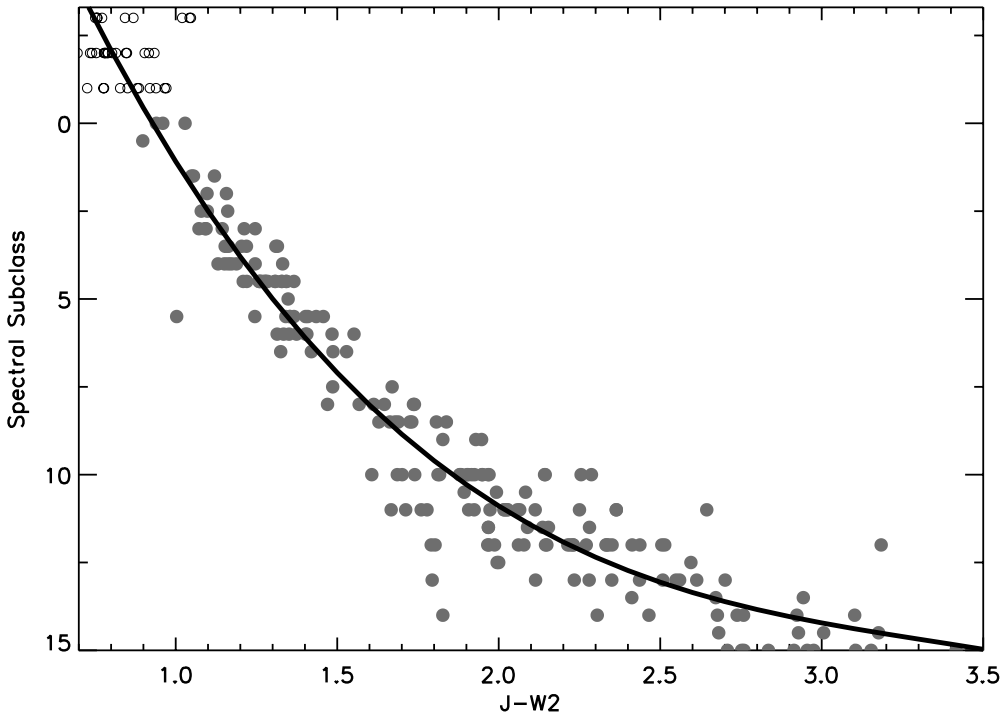

Figure 4. Empirical spectral type relationship derived using *WISE*–2MASS photometry and MLT-dwarfs from Kirkpatrick et al. (2011). On the ordinate, 0 = M0, 5 = M5, 10 = L0, and so forth. We include K-dwarfs (open circles; –1 = K7, –2 = K5, –3 = K4) from Stauffer et al. (2010). We expect our *GALEX* sources to be mainly M dwarfs and anticipate finding few or no bonafide UV-emitting L dwarfs (see Section 2.3). The solid line is Equation (2) and applies best for late K to late M spectral types; see Section 2.3 for details.

2.3. Spectral Types and Distance Estimates

Recently, Kirkpatrick et al. (2011) presented a list of M, L, and T-dwarfs identified with *WISE*. We have used their sample and the *WISE*–2MASS photometry to derive an empirical relationship tying $J - W2$ color to spectral type:

$$\mathrm{SpNum} = -20.039 + 28.402 \times (J - W2) - 8.084 \times (J - W2)^2 + 0.808 \times (J - W2)^3. \quad (2)$$

SpNum is the number past M0, so 0 = M0, 5 = M5, 10 = L0, and so forth (valid from K5/7–L5). Figure 4 shows the Kirkpatrick et al. (2011) sources and our empirical relationship, which works best at spectral types late-K to late-M. We note that this relationship is not valid for L types later than ∼L5 and thus impose a color limit of $W1 - W2 < 0.6$, which selects objects earlier than L5. Despite this limit, we do not anticipate identifying a substantial number of bonafide UV-bright L-dwarfs: we have examined a list of 51 L-dwarf candidates within 40 pc (from Kirkpatrick et al. 2008) with *GALEX* and find that, although 41 of them lie in *GALEX*-covered regions, none are detected. Similar results are found when searching among L and T dwarfs listed at DwarfArchives.org.

Candidates identified in the present program have spectral types predominantly in the M3–M5 range, as estimated from the relationship above. These spectral types are, in general, accurate to ±1 subclass in the early- to mid-M dwarf range, as we demonstrate in Section 3.3. While some studies have presented redder colors for young L-dwarfs compared to older field dwarfs (see Faherty et al. 2013 and references therein), this may not be the case for the M-dwarf spectral types we are sensitive to or to the $J - W2$ colors we use (see, for example, Lyo et al. 2004). Warm circumstellar material in the system can produce more emission in the *WISE* bands and thus make an object redder in $J - W2$ color, mimicking a later spectral type. A visual extinction of 1 mag, either due to a dusty disk or the intervening interstellar medium, would result in $J - W2$ colors redder by about 0.2–0.3 mag (Cardelli et al. 1989). As can be seen in Figure 4, an M5 dwarf, for example, may appear as an M7 or M8 given 1 mag of visual extinction toward the star. Given the relative proximity of these stars to Earth, extinctions this high are more likely due to dust within the system. Note, however, that 1 mag of visual extinction would result in 2.96 mag of extinction at NUV wavelengths (Cardelli et al. 1989), which might, in many or even most cases, lower the apparent UV excess and thereby remove an M-dwarf from consideration as young (given our selection criteria). Thus, in general, we expect GALNYSS sample objects with unusually late inferred spectral types to be dusty systems wherein a disk contributes to the system's mid-IR emission without obscuring the star.

Given that the ages of our candidates are unknown, we compute distances using two empirical isochrones, one for an age of ∼10 Myr and the other for an age of ∼100 Myr. These isochrones are determined from known young, moving group stars (Figure 5). Figure 5 displays absolute *K*-band magnitude versus $J - W2$ color and shows members of the TWA (Schneider et al. 2012a) and other local groups, with ages ∼ 10 Myr (Torres et al. 2008), alongside Pleiades candidates from Stauffer et al. (2007) and cool field dwarfs (ages >100 Myr) from Dupuy & Liu (2012) and Faherty et al. (2012). A piecewise polynomial fit was performed for the ∼10 Myr old stars and subsequently shifted down to match the locus of low-mass Pleiades stars. For this work we adopt our ∼100 Myr old empirical isochrone given the greater agreement with the low-mass population of the Pleiades and its estimated age of 100–125 Myr (Stauffer et al. 2007 and references therein). The theoretical 100 Myr NextGen isochrone dips down into the old (>100 Myr) population for $J - W2 > 1.3$. We note that our empirical ∼10 Myr old isochrone agrees within ∼0.5 mag with the NextGen theoretical

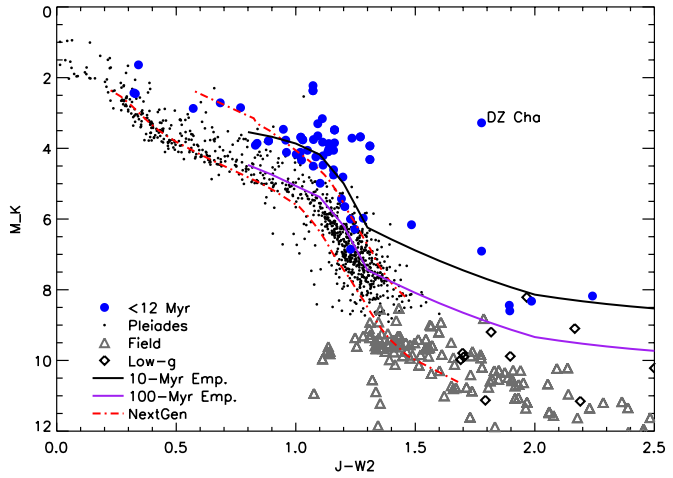

Figure 5. Empirical ∼10 and ∼100 Myr isochrones derived for known young stars listed in Torres et al. (2008) and Schneider et al. (2012a). NextGen models of the same age are shown for comparison (Hauschildt et al. 1999; see http://phoenix.ens-lyon.fr/Grids/NextGen/). Pleiades star data are drawn from Stauffer et al. (2007), data for the field (ages > 100 Myr) population of low-mass dwarfs are drawn from Dupuy & Liu (2012) and Faherty et al. (2012), and data for low-gravity objects come from Faherty et al. (2012). The red end of the ∼10 Myr isochrone (near $J - W2 = 2$) is constrained only by TWA 26, 27, 28, and 29, which are M8–M9 dwarfs; see Section 2.3 for more details.

(A color version of this figure is available in the online journal.)

isochrone over the range $0.8 < J - W2 < 1.3$, corresponding to spectral types ∼M0–M5. A ∼0.5 mag error in the absolute magnitude corresponds to a ∼20% uncertainty in the distance. We thus expect that distances estimated from these isochrones are no more accurate than ∼20%.

Although we extend our isochrones to $J - W2$ of 2.5, this regime is constrained only by a few TWA members, namely, TWA 26, 27, 28, and 29. These are M8–M9 dwarfs with known parallax distances. The isochrones are best constrained at early or mid-M spectral types (i.e., $0.8 < J - W2 < 1.3$) where more stars have been measured. Subsequent work in identifying additional late-M members of these young groups will be key in constraining empirical isochrones and improving on existing theoretical pre-main sequence evolutionary tracks.

2.4. Kinematic Candidate Selection

An important step in confirming membership of candidate stars selected on the basis of their colors and PMs is determination of Galactic space velocities (*UVW*). We define *U* as positive toward the Galactic center, *V* positive in the direction of Galactic rotation, and *W* positive toward the north Galactic pole. Because nearly all candidates lack radial velocities, we use the photometric 10 and 100 Myr distance estimates (as described above) along with the positions and PMs to estimate *UVW* with respect to the Sun for a range of assumed radial velocities extending from −80 to 80 km s^{-1}. Zuckerman & Song (2004) define a "good *UVW* box" that contains nearly all young stars within ∼100 pc of Earth. We have used a somewhat broader version of this box extending to more negative *U* in order to account for members of the Argus association, all of which have $U \sim -22$ km s^{-1} (Torres et al. 2008; Zuckerman et al. 2011; Zuckerman & Song 2012). If, for the range of radial velocity from −80 to +80 km s^{-1}, a star has *UVW* velocities within this acceptable *UVW* range—that is, *U*, *V*, and *W* within 0 to −25, −10 to −34, and +3 to −20 km s^{-1}, respectively—then it is flagged for followup investigation.

When calculating *UVW* velocities, we consider three estimates of PMs: PPMXL, UCAC4, and our *WISE*/2MASS estimates. We calculate *UVW* based on each of these three PM lists individually and then retain only those that lie within the acceptable range of *UVW* for young stars. For approximately one-third of the sample, the PMs from all three lists yield a range of acceptable *UVW*; for another third, two of the three lists yield acceptable *UVW*; and for the remaining third, only one list yields some *UVW* entries in the acceptable *UVW* range. Given that nearly all sources have PMs in PPMXL, we favor PPMXL PMs in preference to those of UCAC4 and our own (*WISE*/2MASS-based) estimates. The *UVW* estimation is performed via custom IDL routines, but an online Javascript calculator[8] is available to quickly calculate the potential range of *UVW* velocities for a single star by varying radial velocity or distance choices.

We tested the robustness of this analysis with known young moving group members listed in Torres et al. (2008). For objects with spectral types K5 or later, we calculated distances using our isochrones, gathered PM information, and calculated *UVW* velocities as described above. We find that 92.5% of the Torres et al. (2008) young moving group members are recovered. The resulting ∼10 and ∼100 Myr isochrone distances calculated by our methodology are within 20%–30% of the parallax and kinematic distances listed in Torres et al. (2008).

2.5. Resulting Candidate Nearby, Young M Dwarfs

The steps described in Sections 2.1–2.4 above were performed for the entire *GALEX* GR 4/5 database, resulting in a list of 32,412 sources (use of the GR 6 database, which was released subsequent to our GR 4/5 database search, adds only 2% of new sky coverage). We trimmed the source list by requiring an object's *UVW* velocities be within the acceptable *UVW* box for a radial velocity range of at least 15 km s^{-1} using the ∼10 Myr isochrone distance—that is, at least ∼10% of the full radial velocity range we tested yields *UVW* velocities consistent with young-star status, given the star's adopted PM and assuming an age of 10 Myr. We furthermore required that these sources have ∼10 Myr distance estimates that place them within 150 pc of Earth. After applying these additional constraints, we obtain a list of 2107 candidate nearby, young, low-mass stars.

Despite the greater *GALEX* coverage in the northern hemisphere (∼65% versus ∼57% in the south), more of our ∼2100 *GALEX*-selected nearby, young, low-mass stars lie in the southern sky (58% versus 42% in the north). These results are consistent with a preponderance of young moving groups in the south, as noted previously by Zuckerman & Song (2004) and Torres et al. (2008). Given our identification of ∼850 northern young star candidates, the present work may lead to the identification of potential new young moving groups in the northern hemisphere.

With Equation (2), we estimate spectral types for all 2107 candidates. One surprising result is an apparent population of UV-bright sources with very late spectral types extending into the L-dwarf regime. As noted in Section 2.3 and further demonstrated in Section 3.3, IR excesses due to warm dust can produce redder $J - W2$ colors than expected, and thus Equation (2) may misclassify dusty systems toward later spectral types. Examining these late-type candidates visually and with SIMBAD revealed that blended sources and carbon stars are also potential

[8] For the *UVW* Javascript calculator, see http://www.astro.ucla.edu/~drodrigu/UVWCalc.html.

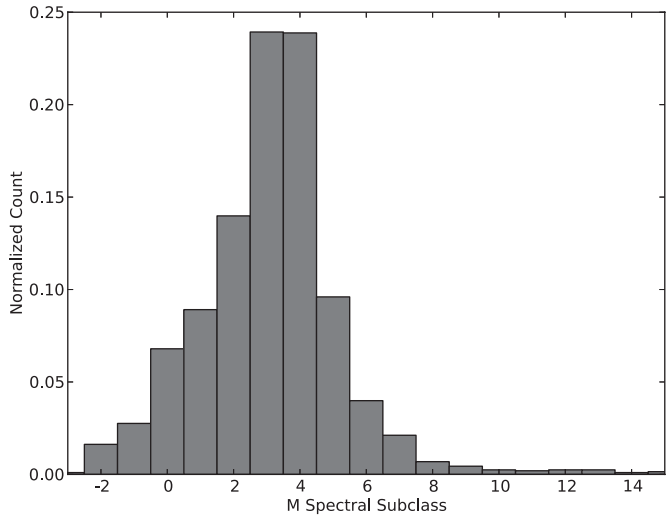

Figure 6. Distribution of photometrically estimated spectral types for our sample of 2031 candidates. The numbers on the abscissa indicate the class past M0, so 0 = M0, 10 = L0, and so forth. We interpret −1 and −2 as indicating spectral types of K7 and K5, respectively (see Sections 2.3 and 2.5 for details).

sources of contamination. However, the dominant contaminant for these late-type objects are galaxies. Such contaminants tend to appear around R.A. and decl. coordinates of approximately (280, 30) and (100, −30) deg, corresponding to the solar apex and antapex. These regions require low PMs and moderately large negative or positive radial velocities (±(20–40) km s^{-1}) in order to match the good *UVW* box described in Section 2.4. We have visually inspected the list of 87 potentially misclassified L-dwarfs and removed 55 galaxy contaminants and 8 blended sources. In addition, we have cross correlated against SIMBAD and removed an additional 13 known galaxies from the full table. The final result is a table of 2031 candidate low-mass stars, with perhaps a few percent contamination from other types of objects.

The distribution of spectral types is shown in Figure 6. About half our candidates have spectral types between M3 and M4, which is similar to the observed distribution of stars in the immediate solar neighborhood (i.e., $D \leqslant 20$ pc; see Figure 7 in Farihi et al. 2005; also Henry et al. 2006; Reid et al. 2007; Bochanski et al. 2010; Stelzer et al. 2013 and references therein). This suggests that our list of 2031 nearby young star candidates likely includes the missing M3–M5 members of nearby, young moving groups. Further work will be necessary to see if any bonafide L-dwarfs or dusty M-type stars are also present in our sample.

Rather than publishing the present, full list of 2031 GALNYSS candidates, the vast majority of which remain unconfirmed, we have elected here to focus on a subset of this list (Section 3), to demonstrate the basic characteristics of the objects we are identifying. The full GALNYSS table will be presented in a future publication.

2.6. Spectroscopic Followup

In order to confirm that the candidates identified via the methods of Sections 2.1–2.5 are in fact young low-mass stars, we must follow up with spectroscopic observations designed to exploit diagnostics of youth. Candidates considered for spectroscopic followup in this and forthcoming papers are those with a broad range of radial velocities that would give *UVW* velocities consistent with nearby, young star status.

Low to medium-resolution spectroscopy can be used to confirm spectral types and identify features of youth. Emission lines from hydrogen and helium can indicate stellar activity common to young stars (White & Basri 2003), while the strength of Na I absorption lines can indicate low surface gravity (Lawson et al. 2009; Schlieder et al. 2012a and references therein) and, thus, pre-main sequence star status. Lithium absorption at 6708 Å is also a widely used diagnostic for youth. However, lithium has been shown to be rapidly depleted within ∼10 Myr or so for mid-M stars (Song et al. 2002; Zuckerman & Song 2004; Yee & Jensen 2010). Thus the absence of Li absorption only demonstrates that a mid-M star is older than ∼10 Myr. At IR wavelengths, a triangular (or "peaky") shape to the *H*-band profile and weak FeH, Na I, and K I features are all indicative of low surface gravity for late-M dwarfs (Lucas et al. 2001; Allers et al. 2007; Rice et al. 2010; Faherty et al. 2013). With high spectral resolution, radial velocities can be measured for our candidate stars. The radial velocity can then be used to constrain the *UVW* velocity so as to solidify young star status and perhaps place a system among known moving groups.

3. GALNYSS IDENTIFICATION OF NEARBY, YOUNG, LOW-MASS STARS IN THE TUCANA–HOROLOGIUM ASSOCIATION

The Tucana–Horologium association (Tuc–Hor) was independently identified by Zuckerman & Webb (2000) and Torres et al. (2000), originally as two separate nearby moving groups. Zuckerman et al. (2001) later suggested that these two groups be merged into a single group located ∼50 pc from the Earth. Subsequent studies (see Zuckerman et al. 2011; Zuckerman & Song 2012 and references therein) have proposed additional stars as members of the group. Malo et al. (2013) list 44 bona fide members (of a possible 67) with distances ranging from 36–71 pc. An age of 10–40 Myr (Zuckerman & Webb 2000) and ∼30 Myr (Torres et al. 2000) has been proposed for Tuc–Hor members based on the strength of Hα emission, Li abundance, X-ray emission, and stellar isochrones (see also Section 2.3.1 in Malo et al. 2013). For purposes of this paper, we have used the 44 Tuc–Hor members listed in Torres et al. (2008) and have adopted an age of ∼30 Myr and group distance of ∼50 pc.

We have applied the methods described in Section 3.1 to our list of ∼2000 GALNYSS-identified nearby young star candidates, and have identified a list of 58 candidates in the vicinity of Tuc–Hor whose kinematics are consistent with membership in this association. We note, however, that given the similarity in the *UVW* of members of Tuc–Hor and the ∼30 Myr old Columba association (Torres et al. 2008), some of these candidates may instead be members of Columba (Section 3.5).

3.1. F-value Analysis

The large number of candidate nearby, young stars yielded by GALNYSS complicates searches for numerically sparse but kinematically coherent groups of candidates in specific search regions such as Tuc–Hor. Hence, we devised a method to group together objects with similar PMs and distance estimates. This involves the calculation of a quantity, which we call F, for a given star among a sample of stars in some region of the sky:

$$F = \sqrt{\left(\frac{\mu_{\rm ra}}{\mu_{\rm ra,0}} - 1\right)^2 + \left(\frac{\mu_{\rm dec}}{\mu_{\rm dec,0}} - 1\right)^2 + \left(\frac{d}{d_0} - 1\right)^2}.$$

The $(\mu_{\rm ra,0}, \mu_{\rm dec,0}, d_0)$ terms correspond to the averages in PM and distance from Earth of the group of stars being compared.

For simplicity, uncertainties in these terms are not folded into this expression. Stars can be either members of a known group, such as the TWA, or all GALNYSS sources in a selected area of the sky. Objects within a chosen threshold F-value are retained as candidate group members and considered for follow up study. For applications of the F-value analysis to an arbitrary region of the sky (i.e., not using an already known moving group to provide the average terms), we perform the analysis in an iterative fashion by selecting a threshold F_T and rejecting sources that have F-values larger than adopted cutoffs of $2.5 \times F_T$, $1.25 \times F_T$, and F_T, and then recomputing the average ($\mu_{\rm ra,0}$, $\mu_{\rm dec,0}$, d_0) terms for each step using sources that were not rejected.

To validate this technique, we applied the F-value analysis to members of the TWA, to Tuc–Hor, and to random fields in the GALNYSS candidate table. For the 26 TWA members listed in Schneider et al. (2012a) with measured PMs, we find average parameters and standard deviations of ($\mu_{\rm ra} = -78 \pm 22$ mas yr^{-1}, $\mu_{\rm dec} = -24 \pm 9$ mas yr^{-1}, $d = 53 \pm 17$ pc) and F-values ranging from above 0 up to 1.2. The two largest F-values (1.1 and 1.2) are found for TWA 12 and 31, both of which have been considered questionable members of the TWA (see Schneider et al. 2012a). The remaining objects have F-values smaller than unity. Tuc–Hor, on the other hand, shows a much broader F-value distribution, with values up to 2.2. The average terms for the members listed in Torres et al. (2008) are ($\mu_{\rm ra} = 73 \pm 24$ mas yr^{-1}, $\mu_{\rm dec} = -36 \pm 32$ mas yr^{-1}, $d = 49 \pm 9$ pc).

In contrast, when examining random groups of *GALEX* young star candidates, we find much larger F-values (in some cases, $F \sim 100$). This suggests that F-value thresholds of a few are adequate to select objects that may be members of young groups like TWA and Tuc–Hor. We note that the F-value technique will not work efficiently in well-dispersed stellar moving groups, such as the β Pic moving group, where members possess a wide range of PMs and distances from Earth or when members lie near the location of a group's convergent point. However, it can still be applied in small regions for such groups.

We applied this F-value technique to the 2031 candidate nearby young stars (Section 2.5) to investigate the potential presence of young groups of stars at random locations across the sky. Candidate groups are generated by selecting stars that lie within 20–30 deg of a chosen location and applying the iterative method described above. One of the largest groups so identified is coincident with the location of most known Tuc–Hor members. This group of 58 stars (listed in Table 2) was identified considering a search radius of 30 deg centered at (45, −45) deg. The mean PMs of the stars in Table 2 (73 ± 22, -14 ± 13 mas yr^{-1}) match those of known Tuc–Hor members (see above) reasonably well (Figure 7), despite our exclusion of known Tuc–Hor members to determine these values of $\mu_{\rm ra,0}$, $\mu_{\rm dec,0}$, and d_0. The F-values listed in Table 2 range up to 2, similar to those of known Tuc–Hor members. Indeed, the distributions of F-values for candidates and for known members are indistinguishable from each other, as shown by a K-S test ($P = 0.79$). In contrast, comparing the distributions of either Table 2 Tuc–Hor candidates or known Tuc–Hor members with that of TWA members yields K-S test $P =$ few $\times 10^{-3}$, consistent with different underlying F-value distributions for TWA and Tuc–Hor. Most Table 2 candidates, if at the ∼30 Myr age of Tuc–Hor, have distances close to ∼50 pc, in agreement with the known Tuc–Hor members. We stress that most of these objects are only candidates at this stage in our work.

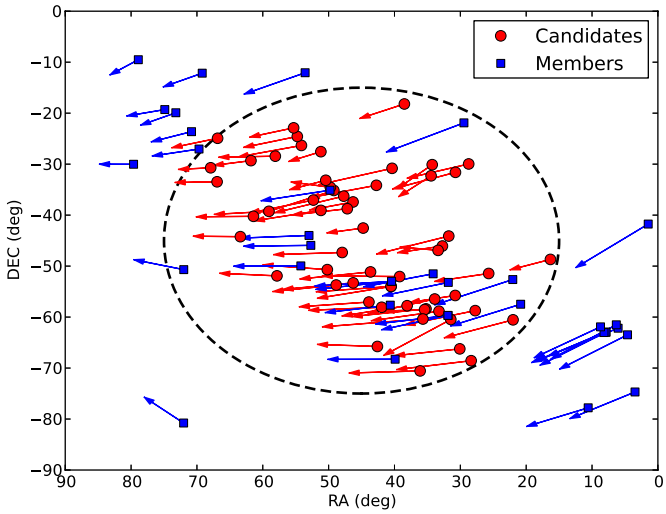

Figure 7. Proper motions for the 58 young, low-mass candidates (see Table 2) compared with those of known Tuc–Hor members (Torres et al. 2008). The dashed line highlights the region considered in this study (see Section 3.1).
(A color version of this figure is available in the online journal.)

Furthermore, additional Tuc–Hor candidates likely exist beyond the region we have searched and are not considered in this paper. In Sections 3.3–3.6, we discuss properties of the Table 2 candidates, and in fact are able to rule out Tuc–Hor membership for some of them. Note that, although these rejected candidates are unlikely to be Tuc–Hor members, they may be members of other moving groups (e.g., β Pic, Columba, or AB Dor) and, hence, may still be young (age < 100 Myr) stars.

3.2. Convergent Point Analysis

To complement the F-value analysis described in Section 3.1, we also performed a convergent point analysis on the candidate Tuc–Hor members. The convergent point analysis methodology has been described in detail elsewhere (Mamajek 2005; de Bruijne 1999; Jones 1971); here, we have applied a simplified algorithm. This analysis consists of selecting a convergent point location and determining the PMs ($\mu_\perp$) perpendicular to the great circle connecting a star to the convergent point. The typical analysis removes suggested but discrepant members from a list until the convergent point analysis passes some threshold. We have simplified the procedure by neglecting this step; that is, we retain potentially discrepant members while determining the location of the convergent point. This simplification, combined with the coarse, 1 degree grid we use for convergence point calculations, likely results in a convergent point that is less accurate than would be obtained for a more rigorous treatment in which outliers are rejected. However, the simplified algorithm is sufficient for the purposes of this work, namely, identifying candidate new members of moving groups.

Given a convergent point location for a moving group and the perpendicular motion of a candidate group member, one can estimate a membership probability:

$$P = \exp\left(-\frac{1}{2}\frac{\mu_\perp^2}{\left(\sigma_\perp^2 + \sigma_{\rm int}^2\right)}\right).$$

The quantity $\sigma_\perp$ incorporates error terms in the PM and convergent point location (Equation (12) in de Bruijne 1999), while $\sigma_{\rm int}$ accounts for the internal dispersion in the group.

Table 2
Candidate Young Stars

Index	*WISE* Designation	$\mu_{\rm R.A.}$ (mas yr^{-1})	$\mu_{\rm decl.}$ (mas yr^{-1})	$\mu_{\rm tot}$ (mas yr^{-1})	PM Source	Est. Sp. Type[a]	*F*-value
1	J010516.16−484116.9	46.8 ± 1.7	−15.6 ± 1.7	49.3	UCAC4	M5.5	1.55
2	J012758.87−603224.5	89.9 ± 3.1	−30.4 ± 2.9	94.9	UCAC4	M4.1	1.04
3	J014246.89−512646.9	66.8 ± 4.2	−12.7 ± 4.2	68.0	UCAC4	M6.7	0.68
4	J015057.01−584403.4	92.2 ± 2.0	−24.3 ± 2.0	95.3	UCAC4	M2.8	1.59
5	J015325.09−683322.8	98.0 ± 2.9	−15.1 ± 2.4	99.2	UCAC4	M5.2	0.36
6	J015455.24−295746.0	78.7 ± 2.0	−23.6 ± 1.4	82.2	UCAC4	M5.2	0.79
7	J020020.08−661402.0	84.0 ± 6.3	−11.4 ± 3.4	84.8	UCAC4	M4.4	0.68
8	J020257.94−313626.4	81.0 ± 2.9	−27.7 ± 2.3	85.6	UCAC4	M4.7	0.47
9[b]	J020306.68−554542.1	54.2 ± 25.0	−10.7 ± 25.0	55.2	*WISE*-2M	M4.5	0.48
10	J020547.70−602808.4	89.1 ± 1.5	−61.7 ± 1.5	108.4	UCAC4	M5.0	0.39
11	J020701.85−440638.3	94.9 ± 1.3	−30.6 ± 1.3	99.7	UCAC4	M3.3	1.57
12[c]	J021053.50−460351.4	53.2 ± 1.8	−10.2 ± 1.8	54.2	UCAC4	M4.3	0.82
13	J021258.28−585118.3	87.7 ± 1.3	−15.9 ± 1.3	89.1	UCAC4	M2.8	0.38
14	J021330.24−465450.3	42.5 ± 1.0	4.9 ± 1.0	42.8	UCAC4	M3.8	1.07
15	J021533.37−562717.6	86.4 ± 17.1	−24.7 ± 17.1	89.8	PPMXL	M7.5	0.83
16	J021705.03−300621.9	40.7 ± 4.5	−36.1 ± 4.0	54.4	UCAC4	M4.6	1.26
17	J021745.82−321718.2	37.4 ± 13.4	−31.0 ± 0.9	48.6	UCAC4	M0.7	0.56
18	J022051.50−582341.3	97.3 ± 2.0	−13.0 ± 2.0	98.2	UCAC4	M3.2	0.62
19	J022142.84−583204.4	46.4 ± 2.4	−2.2 ± 2.4	46.5	UCAC4	M3.5	0.83
20	J022244.32−602247.7	137.4 ± 1.7	−13.8 ± 1.7	138.1	UCAC4	M3.8	1.04
21	J022424.69−703321.2	92.5 ± 2.7	−3.6 ± 3.9	92.6	UCAC4	M4.3	0.35
22	J023219.44−574611.9	83.8 ± 2.3	−17.1 ± 2.6	85.5	UCAC4	M4.7	0.29
23	J023359.89−181152.5	53.5 ± 1.7	−22.5 ± 1.7	58.0	UCAC4	M3.7	1.24
24	J023651.80−520303.5	102.2 ± 0.8	1.2 ± 0.8	102.2	UCAC4	M2.6	0.85
25	J024127.29−304915.1	97.0 ± 2.1	−28.0 ± 2.2	101.0	UCAC4	M4.6	0.91
26	J024202.14−535914.7	97.0 ± 2.1	−20.2 ± 2.2	99.1	UCAC4	M4.5	0.20
27	J024204.15−535900.0	98.4 ± 2.2	−9.1 ± 7.6	98.8	UCAC4	M4.8	0.47
28	J024746.49−580427.4	95.5 ± 1.4	−5.2 ± 3.5	95.6	UCAC4	M2.9	0.94
29	J025022.35−654555.2	75.8 ± 1.9	3.4 ± 1.9	75.9	UCAC4	M3.4	1.26
30	J025059.67−340905.3	87.2 ± 1.8	−21.0 ± 1.8	89.7	UCAC4	M4.6	1.06
31	J025433.25−510831.4	92.0 ± 1.2	−11.9 ± 1.2	92.8	UCAC4	M3.1	0.47
32	J025531.87−570252.3	90.5 ± 2.7	−8.0 ± 2.8	90.9	UCAC4	M4.2	0.70
33	J025901.49−423220.4	39.9 ± 4.1	−6.9 ± 4.4	40.5	UCAC4	M7.4	0.55
34	J030505.65−531718.4	91.4 ± 3.6	−11.0 ± 3.6	92.1	UCAC4	M4.8	1.04
35	J030509.79−372505.8	50.8 ± 1.3	−12.2 ± 1.3	52.2	UCAC4	M2.5	0.66
36	J030839.55−384436.3	68.7 ± 3.2	−10.1 ± 4.2	69.4	UCAC4	M4.2	0.64
37	J031049.48−361647.3	90.4 ± 1.9	−28.1 ± 1.9	94.7	UCAC4	M4.3	0.37
38	J031145.52−471950.2	88.9 ± 1.8	−3.6 ± 2.0	89.0	UCAC4	M4.5	0.68
39	J031523.72−534253.9	81.0 ± 9.5	−10.8 ± 7.2	81.7	UCAC4	M5.2	1.20
40	J031650.45−350937.9	92.3 ± 1.1	−38.3 ± 1.1	99.9	UCAC4	M3.7	0.79
41	J031856.73−343317.6	44.5 ± 2.6	7.9 ± 2.8	45.2	UCAC4	M4.3	0.96
42	J032047.66−504133.0	82.6 ± 1.7	7.8 ± 1.5	83.0	UCAC4	M2.2	1.68
43	J032144.76−330949.5	40.5 ± 3.1	−13.6 ± 3.1	42.7	UCAC4	M6.0	1.16
44	J032440.63−390422.8	86.3 ± 1.9	−17.4 ± 1.6	88.0	UCAC4	M4.2	0.56
45	J032443.06−273323.1	34.4 ± 3.9	−13.6 ± 3.9	36.9	PPMXL	M9.2	0.54
46	J032916.57−370250.2	82.2 ± 2.6	−21.6 ± 2.2	85.0	UCAC4	M4.4	0.31
47	J033631.50−261958.1	81.0 ± 4.0	−19.0 ± 4.0	83.2	UCAC4	M5.7	0.98
48	J033901.64−243406.1	66.7 ± 2.6	−17.6 ± 2.7	69.0	UCAC4	M6.0	0.41
49	J034115.60−225307.8	51.9 ± 2.3	−14.2 ± 1.6	53.8	UCAC4	M1.4	0.74
50	J035122.95−515458.1	71.7 ± 1.8	4.2 ± 1.8	71.8	UCAC4	M4.2	0.46
51	J035223.52−282619.6	70.5 ± 1.0	−1.7 ± 1.0	70.5	UCAC4	M2.0	1.01
52	J035616.31−391521.8	67.7 ± 2.2	−4.9 ± 2.2	67.9	UCAC4	M4.2	0.06
53	J040539.68−401410.5	71.6 ± 2.0	−0.8 ± 2.1	71.6	UCAC4	M4.2	0.89
54	J040711.50−291834.3	42.0 ± 1.1	−6.9 ± 1.0	42.6	UCAC4	M1.0	0.84
55	J041336.14−441332.4	56.2 ± 1.7	0.7 ± 2.1	56.2	UCAC4	M3.9	0.59
56	J042726.28−245527.4	54.8 ± 3.9	−14.6 ± 3.9	56.7	PPMXL	M4.5	0.50
57	J042745.66−332742.6	48.4 ± 3.3	−1.0 ± 4.7	48.4	UCAC4	M4.5	1.00
58	J043138.61−304250.9	33.7 ± 1.4	−2.2 ± 1.4	33.8	UCAC4	M3.5	0.80

Notes. Candidate young, low-mass stars selected with the *F*-value analysis (see Section 3.1) in the vicinity of Tuc–Hor.
[a] Spectral types estimated from $J - W2$ color (see Section 2.3).
[b] PPMXL and UCAC4 proper motions for J0203−55 differ substantially; we use *WISE*–2MASS estimated proper motions.
[c] J0210−46 is a low-mass companion to AB Dor member CD−46 644 (see the Appendix).

Table 3
Convergent Point Estimates for Several Young Moving Groups within 100 pc of the Earth

Moving Group	Conv. Point R.A.	Conv. Point Decl.	Velocity (km s^{-1})	Distance (pc)	σ_{int} (km s^{-1})
Tuc–Hor	119	−27	23.3	50	1
β Pic	90	−28	20.8	40	1
AB Dor	92	−47	31.2	50	2
TWA	95	−26	21.6	50	1
Carina-Near	98	0	31.3	30	3
Columba	106	−30	26.5	80	1

Notes. The listed velocities are the total space motion with respect to the Sun. These values can be used to estimate membership probabilities, kinematic distances, and radial velocities as described in Section 3.2. We adopt a 2 deg uncertainty on the convergent point location for all groups (Section 3.2). As described in Mamajek (2005), the information returned from the convergent point analysis is not particularly sensitive to group distance and internal dispersion (σ_{int}). We note that the TWA convergent point listed here is somewhat different than that used in Looper et al. (2010; 99.8, −27.7 deg with 22.0 km s^{-1} full space velocity). Carina-Near members are drawn from Zuckerman et al. (2006); the others are from Torres et al. (2008), Zuckerman et al. (2011), and Schneider et al. (2012a).

Given our coarse determination, we adopt an uncertainty of 2 deg for the convergent point location. While the quantitative probabilities so derived may be approximate, they nevertheless present a qualitative estimate of membership probability given an object's PM and the estimated convergent point location of a group.

We have applied this convergent point analysis to the known members of Tuc–Hor listed in Torres et al. (2008). We determine a convergent point of (119, −27) deg for Tuc–Hor and used PMs, distances (both parallax and kinematic; Torres et al. 2008), and radial velocities (Torres et al. 2006) to determine a mean total heliocentric space velocity magnitude of 23.3 ± 1.3 km s^{-1} (Table 3); here the quoted error is the standard deviation of the velocities. We thus adopt an internal velocity dispersion (σ_{int}) of 1 km s^{-1} and, given the known member distance distribution, a group distance of 50 pc in our analysis. The group distance is used to convert the velocity dispersion in km s^{-1} to mas yr^{-1} (with the result 4 mas yr^{-1} for Tuc–Hor). However, the convergent point location is not very sensitive to these estimates (see Mamajek 2005).

The space velocity of known members can be combined with the angular distance between a given target star and the convergent point to estimate the radial velocity and distance the target would have if it were a member. We have created an online Javascript calculator for this purpose.[9] Table 3 lists convergent point information for various groups determined via the method described above. These can be used as inputs for our Javascript tool.

The kinematic distance and radial velocity estimates for the 58 Tuc–Hor candidates (Table 2) are tabulated, along with the probabilities described here, in Table 4. In Figure 8, we use our kinematic distances to construct a color–magnitude diagram for the candidate Tuc–Hor stars. The Tuc–Hor low-mass candidates lie above the IC2391 members in the color–magnitude diagram,

[9] The online calculator takes, as inputs, moving group convergence point data and stellar coordinates and proper motions, and outputs the membership probability as well as expected kinematic distance and radial velocity the star would have as a member of the group of interest; see http://www.das.uchile.cl/~drodrigu/CPCalc.html.

Table 4
Membership Probabilities for Table 2 Sources

ID	This Work			BANYAN[a]		
	Prob (%)	RV (km s^{-1})	Dist. (pc)	Prob (%)	RV (km s^{-1})	Dist. (pc)
J0105−48[b]	30.2	4.9	98.1	0.0	6.0	...
J0127−60	95.8	7.9	48.5	97.9	8.9	46.5
J0142−51[b]	23.6	7.5	69.0	16.9	8.5	55.0
J0150−58	95.4	8.8	47.5	96.8	9.7	45.5
J0153−68	79.0	9.7	44.9	99.0	10.6	44.0
J0154−29[b]	15.0	5.2	58.5	8.4	6.3	49.5
J0200−66	78.8	9.8	52.4	98.4	10.7	49.5
J0202−31[b]	60.7	6.1	55.3	20.5	7.1	48.5
J0203−55[b]	99.1	9.1	81.7	8.3	10.0	60.0
J0205−60[b]	0.0	9.6	44.5	0.5	10.5	...
J0207−44	98.7	8.0	46.0	98.5	9.1	43.5
J0210−46[b]	49.5	8.5	84.5	0.2	9.6	...
J0212−58	95.3	9.8	49.8	96.3	10.8	47.0
J0213−46[b]	0.1	8.8	115.0	0.0	9.8	...
J0215−56	94.0	9.8	49.6	94.9	10.7	46.5
J0217−30[b]	1.0	6.9	91.3	0.0	8.0	...
J0217−32[b]	6.2	7.3	101.0	0.0	8.3	...
J0220−58	78.3	10.1	44.9	95.7	11.1	43.5
J0221−58[b]	54.0	10.2	95.4	0.4	11.1	...
J0222−60	57.6	10.3	31.8	65.1	11.3	32.5
J0224−70	98.0	10.8	46.8	99.6	11.6	46.0
J0232−57	65.5	10.6	50.9	95.2	11.6	47.5
J0233−18[b]	98.5	6.5	80.9	0.0	7.5	...
J0236−52[b]	0.3	10.6	43.4	60.6	11.5	41.0
J0241−30	69.8	8.9	44.8	59.4	9.9	42.5
J0242−53W	54.7	10.9	43.6	92.0	11.9	42.0
J0242−53E	87.9	10.9	43.7	96.5	11.9	42.5
J0247−58	92.3	11.4	44.6	95.0	12.3	43.5
J0250−65	85.4	11.6	55.9	97.5	12.4	51.5
J0250−34	70.2	10.0	49.3	58.1	10.9	45.5
J0254−51	99.9	11.5	45.8	97.0	12.4	44.0
J0255−57	93.3	11.7	46.5	94.6	12.6	44.5
J0259−42[b]	98.6	11.3	105.7	0.0	12.2	...
J0305−53	77.1	12.1	45.4	92.9	13.0	43.5
J0305−37[b]	99.8	11.3	81.9	0.6	12.2	...
J0308−38[b]	78.7	11.6	61.1	23.8	12.5	52.0
J0310−36	48.6	11.6	44.9	95.9	12.5	43.0
J0311−47	52.2	12.3	46.8	91.8	13.2	44.0
J0315−53	63.5	12.6	50.5	86.6	13.5	46.5
J0316−35[b]	1.2	11.9	42.6	93.4	12.8	40.5
J0318−34[b]	0.3	12.0	100.8	0.0	12.9	...
J0320−50[b]	9.3	12.9	49.5	71.8	13.7	45.5
J0321−33[b]	80.0	12.1	98.1	0.0	13.0	...
J0324−39	88.8	12.7	46.6	94.4	13.6	44.0
J0324−27[b]	86.6	11.8	114.5	0.0	12.6	...
J0329−37	51.7	12.9	48.0	95.0	13.7	45.0
J0336−26[b]	76.2	12.5	49.6	44.1	13.3	46.5
J0339−24[b]	84.8	12.5	59.7	19.1	13.3	52.5
J0341−22[b]	84.6	12.5	76.6	1.2	13.3	59.5
J0351−51	97.6	14.4	53.3	93.3	15.2	49.0
J0352−28[b]	0.9	13.9	57.0	20.0	14.6	49.5
J0356−39	97.7	14.7	55.8	65.4	15.4	50.0
J0405−40	87.0	15.3	51.5	68.8	16.0	47.5
J0407−29[b]	90.9	14.9	88.1	0.2	15.6	...
J0413−44	96.9	15.7	64.1	81.4	16.4	54.0
J0427−24[b]	99.6	15.9	62.7	14.8	16.5	55.5
J0427−33[b]	80.8	16.4	71.7	3.6	17.0	57.5
J0431−30[b]	82.6	16.5	102.0	0.0	17.1	...

Notes. Convergent point analysis probabilities, predicted radial velocities, and kinematic distances for our Tuc–Hor candidates (see Table 4). BANYAN does not predict distances for low probability objects.
[a] See Malo et al. (2013).
[b] Possible members of other moving groups or old field dwarfs; see the Appendix.

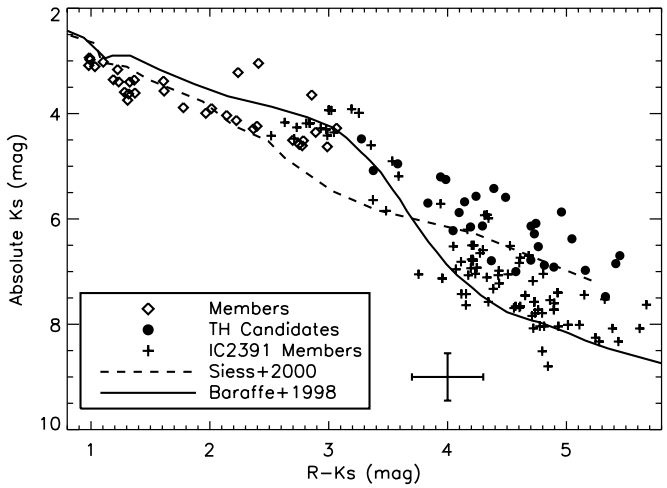

Figure 8. *Ks* vs. $R-Ks$ color–magnitude diagram for previously established Tuc–Hor members and the Table 2 candidate objects. *Ks* magnitudes come from 2MASS; *R* comes from NOMAD, which in turn are drawn from either USNO-B1 or UCAC2. Given that the *R* magnitudes come from separate catalogs, we adopt a 0.3 mag error for $R-Ks$. This is shown as the approximate typical uncertainty (error bar at bottom center), which includes a 20% distance error. For the candidate objects, we use kinematic distances derived in our convergent point analysis (see Section 3.2). We do not show candidates whose properties indicate they may not be Tuc–Hor members (see Section 3.5, the Appendix, and Table 10). For comparison, we show members of the ∼50 Myr old cluster IC2391, located 155 pc from Earth (Barrado y Navascués et al. 2001). Theoretical isochrones for age 30 Myr from Baraffe et al. (1998) and Siess et al. (2000) are also shown. The 3 Tuc–Hor members above the sequence with $R-K$ between 2 and 3 are HD 3221, BD−20 951, and CD−53 544. BD−20 951 is a known spectroscopic binary, while CD−53 544 is a visual double (Torres et al. 2008).

suggesting the Tuc–Hor candidates have ages <50 Myr, consistent with the age of Tuc–Hor as inferred from prior studies (see Section 3). A pair of theoretical 30 Myr old isochrones are also shown (Baraffe et al. 1998; Siess et al. 2000); the agreement is marginally better with the Siess et al. (2000) isochrones for the Tuc–Hor candidates. When compared to the absolute magnitudes of field population M-dwarfs (e.g., Kraus & Hillenbrand 2007), we find that our candidates, when located at the kinematic distances we estimate, are all over-luminous, as expected for young systems.

3.3. Spectroscopic Observations

3.3.1. WiFeS

To investigate the nature of the Tuc–Hor candidates, we used the WiFeS spectrograph at the Siding Springs Observatory 2.3 m telescope to observe some of these systems at resolution ∼3000 or ∼7000. WiFeS (Dopita et al. 2007) is a double-beam, image-slicing integral field spectrograph, and provides a $25'' \times 38''$ field with $0\farcs5$ pixels. Observations over the spectral range 3200–9800 Å were carried out in 2012 September and October. Figure 9 shows the spectra, covering the Hα and Li region, for stars observed thus far. Initial analysis has focused on measurements of Hα emission, lithium absorption at 6707 Å, and sodium absorption at 8200 Å. To derive accurate spectral types, we computed the TiO5 index as described in Reid et al. (1995). We list our measurements in Table 5, including a handful of cases in which published spectroscopy exists in the literature.

Figure 10 compares the spectral types initially estimated with $J-W2$ colors to those derived from the TiO5 index (accurate to ±0.5) for Tuc–Hor candidates and young low-mass candidates from Rodriguez et al. (2011). There is evidently sufficiently good agreement between these spectral type estimation methods that a disagreement—in the sense that $J-W2$ is too red—likely indicates the presence of emission from warm dust grains. Such appears the case for J0215−56, J0259−42, and J0324−27 (see Figure 10). We note that at an age of ∼30 Myr, brown dwarfs are expected to have spectral types later than ∼M6 (Burrows et al. 1997; Baraffe et al. 1998).

3.3.2. SpeX

In addition to optical spectra, near-IR spectra for J0202−31, J0259−42, and J0324−27 were obtained with the SpeX spectrograph (Rayner et al. 2003) on the 3 m NASA Infrared Telescope Facility (IRTF). Observations were carried out on 2012 December 25 and 2013 January 1 (UT) with the spectrograph in prism mode with the 0.5 or $0\farcs8$ slit, resulting in $R = \lambda/\Delta\lambda \approx 100$ over the wavelength range 0.7–2.5 μm (Figure 11). Observations were carried out with an ABBA dither pattern along the slit, with exposure times determined by the target magnitudes. A0V stars observed immediately after each target were used as standards for flux calibration and telluric correction. All data were reduced with SpeXtool version 3.3 (Vacca et al. 2003; Cushing et al. 2004) and standard settings.

At the IRTF, we resolved J0202−31 as a $0\farcs5$ binary; but while guiding, the slit did not remain centered on a single component and instead switched between both stars. Comparison with field dwarf standards shows the combined spectrum of the pair to be an M4, in agreement with the spectral type determined from the optical spectrum—which did not resolve the system—suggesting J0202−31 is an equal mass binary. The SpeX spectrum of J0259−42, which displays a very red $J-W2$ color, indicates a spectral type of M5, also in agreement with the optical spectrum. We do not have an optical spectrum for J0324−27, but its SpeX spectrum indicates it is an M5.5, rather than an M9, as indicated by the $J-W2$ color. As we discuss in the Appendix, both J0259−42 and J0324−27 have *WISE* IR excesses that indicate the presence of circumstellar disks. Both show Br-γ emission and weak Na I absorption, which may indicate youth. However, other features, such as the lack of Li absorption in the optical and the shape of the *H*-band profile (see Section 2.6), are inconclusive. J0202−31 does not show any clear signatures of youth in its near-IR spectrum.

3.3.3. Hα and Li

Equivalent widths (EWs) of Hα emission and Li absorption for some of the Tuc–Hor candidates are listed in Table 5. Uncertainties for the EW measurements are computed by using the rms scatter from a linear fit to the continuum around each line and propagating this with a Monte Carlo method. For non-detections, we quote only the 1σ uncertainties. With the exception of J0315−53, no Table 5 star observed with WiFeS shows clear Li absorption at 6708 Å. This is not surprising as, at the expected ∼30 Myr age of these candidates, lithium should have been depleted for early to mid M-type stars (see Section 2.6). J0315−53 is therefore a noteworthy exception as it has a spectral type near M5 and Li absorption EW of ∼370 mÅ. One possibility is that J0315−53 is a member of the ∼10 Myr β Pictoris moving group. To investigate this possibility, we carried out a convergent point analysis using β Pic members in a similar fashion to those of Tuc–Hor (Section 3.2). However, with our estimated convergent point for the β Pic moving group

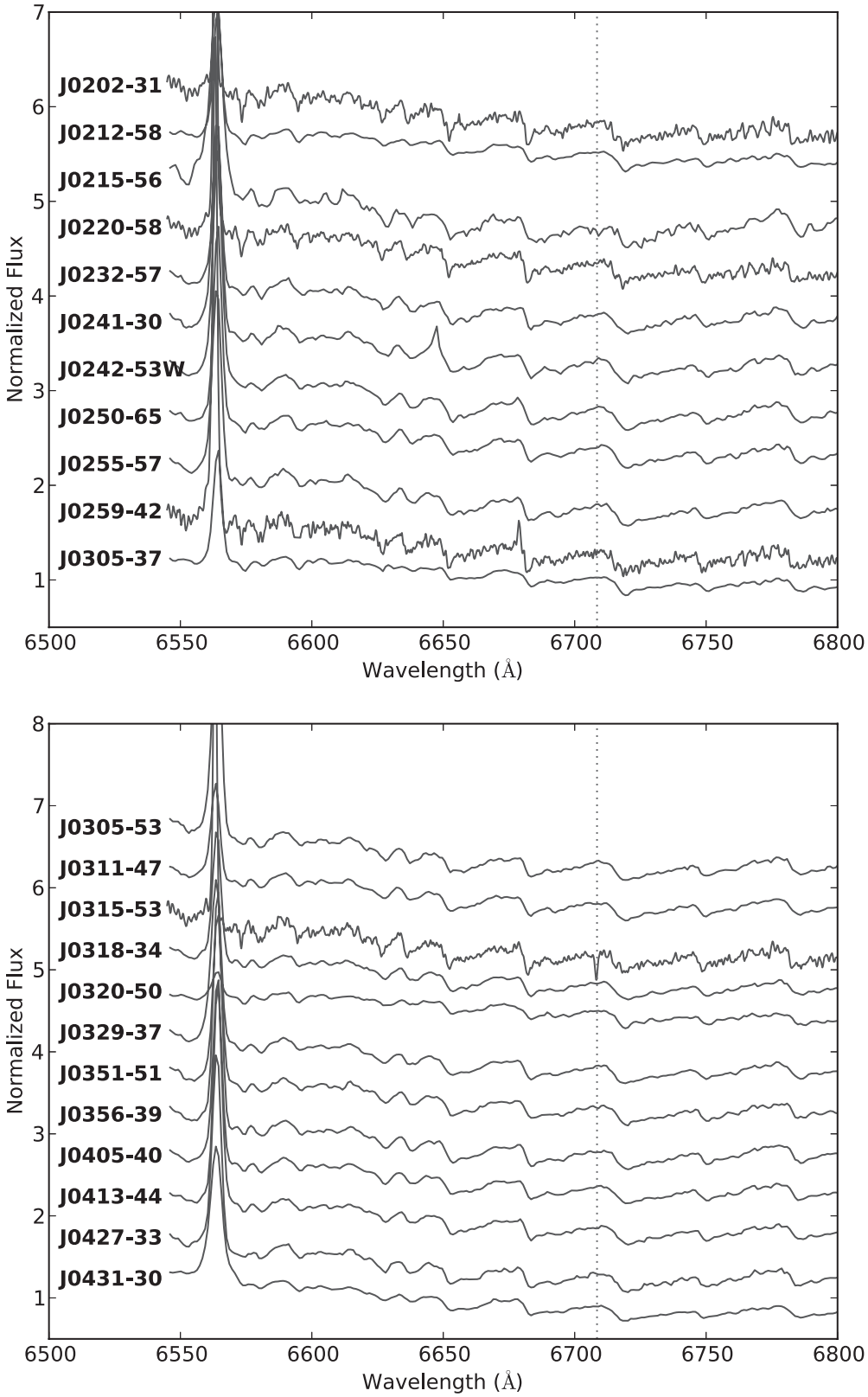

Figure 9. WiFeS spectra for our candidate objects. Spectra for J0202−31, J0220−58, J0259−42, and J0315−53 have $R \sim 7000$, all others have $R \sim 3000$. The vertical line indicates the location of the Li 6708 Å absorption feature; only J0315−53 shows strong Li absorption. The features near 6650 Å for J0241−30 and 6680 Å for J0259−42 are due to uncorrected cosmic ray hits. J0202−31 is a binary system.

(Table 3), we find a probability of only 6% that J0315−53 is a member of β Pictoris (similar to the 0.3% probability returned by the Bayesian analysis of Malo et al. 2013). Hence, while the lithium absorption EW may suggest an age comparable to the β Pic moving group, J0315−53's kinematics nevertheless suggest it is a strong candidate for membership in Tuc–Hor. A handful of Table 2 systems have published spectroscopy available in Riaz et al. (2006) or Torres et al. (2006), including

Table 5
WiFeS Spectroscopic Measurements for Some Table 2 Tuc–Hor Candidates

Object	Sp. Type	Hα EW (Å)	Li EW (Å)	Na I EW (Å)	Na I Index
J0202−31	M4.0	−4.34 ± 0.26	<0.15	4.41 ± 0.32	1.22
J0212−58	M2.1	−4.67 ± 0.27	<0.01	2.92 ± 0.29	1.13
J0215−56	M5.4	−10.29 ± 0.78	<0.03	3.99 ± 0.45	1.20
J0220−58	M3.0	−7.38 ± 0.72	<0.06	...	...
J0232−57	M4.4	−6.07 ± 0.34	<0.05	3.65 ± 0.30	1.16
J0241−30	M4.7	−8.86 ± 0.35	<0.06	3.98 ± 0.36	1.21
J0242−53W	M4.6	−9.65 ± 0.28	<0.05	3.77 ± 0.31	1.19
J0250−65	M3.7	−7.19 ± 0.34	<0.02	3.24 ± 0.29	1.16
J0255−57	M4.9	−7.92 ± 0.33	<0.02	4.14 ± 0.35	1.20
J0259−42	M4.2	−11.01 ± 0.89	<0.11	3.56 ± 0.48	1.17
J0305−37	M1.9	−4.18 ± 0.25	<0.01	2.55 ± 0.23	1.12
J0305−53	M5.4	−10.25 ± 0.43	<0.05	4.17 ± 0.33	1.19
J0311−47	M4.3	−4.51 ± 0.27	<0.04	3.35 ± 0.35	1.17
J0315−53	M5.2	−7.53 ± 0.52	0.37 ± 0.05	3.99 ± 0.37	1.21
J0318−34	M4.1	−5.63 ± 0.32	<0.02	4.38 ± 0.31	1.24
J0320−50	M2.0	−1.28 ± 0.21	<0.03	2.15 ± 0.31	1.11
J0329−37	M4.3	−8.63 ± 0.34	<0.03	3.35 ± 0.36	1.17
J0351−51	M4.4	−7.70 ± 0.44	<0.03	3.71 ± 0.32	1.19
J0356−39	M5.0	−10.01 ± 0.41	<0.04	3.86 ± 0.32	1.19
J0405−40	M4.2	−8.40 ± 0.36	<0.02	3.44 ± 0.31	1.17
J0413−44	M3.9	−9.47 ± 0.35	<0.03	3.37 ± 0.31	1.17
J0427−33	M4.8	−9.63 ± 0.36	<0.04	4.13 ± 0.32	1.21
J0431−30	M3.2	−7.51 ± 0.31	<0.03	3.07 ± 0.36	1.15
J0207−44[a]	M3.5	−4.1	...	...	...
J0213−46[a]	M4	−8.6	...	...	...
J0222−60[a]	M4	−8.1	...	...	...
J0233−18[a]	M3	−8.5	...	...	...
J0236−52[b]	M2	−5.3	0.32	...	...
J0254−51[a]	M1.5	−3.1	...	...	...
J0407−29[a]	M0	−3.2	...	...	...

Notes. We measure equivalent widths (EWs) for Hα, Li, and the sum of the two lines in the Na I doublet at 8183 and 8195 Å. Spectra for J0220−58 were taken with $R \sim 7000$ and do not cover the Na I region. Spectral types are determined using the TiO5 index (Reid et al. 1995) and are accurate to ±0.5. Note that these spectral types can differ from the earlier estimates based on J-W2 colors (see Table 2). The Na I index is the ratio of the average flux on and off the doublet (Figure 13) and is measured in spectra that have been re-binned to $R \sim 800$ (see Section 3.3.4). The final seven systems have measurements published in the literature.
[a] Riaz et al. (2006).
[b] Torres et al. (2006).

J0236−52, another system with clear Li absorption. J0315−53 and J0236−52, among other systems, are considered in more detail in the Appendix.

All Table 5 stars show Hα emission. However, this is not necessarily indicative of youth, as Hα activity can still be seen among old M-dwarfs (West et al. 2008, 2004). West et al. (2008) predict activity lifetimes of the order of ∼1 Gyr for M2 stars and ∼6 Gyr for M6 stars. In fact, M5–M9 stars in the field are commonly seen to show Hα activity, with the latest types nearly always showing activity regardless of age (West et al. 2004). To attempt to determine whether our Hα detections are indicative of ages < 1 Gyr, we make a comparison between our sample and the older sample studied in West et al. (2004). We compute $\log L_{H\alpha}/L_{bol}$ for Table 5 stars as described in Walkowicz et al. (2004). Results are illustrated in Figure 12 along with the average $L_{H\alpha}/L_{bol}$ from West et al. (2004). We find that most of the Table 5 sample have larger $L_{H\alpha}/L_{bol}$ than the field population. This suggests that the Table 5 stars are statistically younger than the field population studied in West et al. (2004). This is not surprising given that we have selected these candidate Tuc–Hor M-dwarfs based on UV emission from *GALEX* which likely originates from the active chromospheres of young stars (see the Introduction).

3.3.4. Sodium as an Indicator of Youth

Several recent studies have shown that Na I absorption can be used as a diagnostic of stellar surface gravity and thus of youth (Schlieder et al. 2012a; Lawson et al. 2009; Mohanty et al. 2004a, 2004b). In particular, young objects are expected to have lower surface gravities and hence weaker Na I absorption. The spectral feature used in these studies is the Na I doublet at 8183 and 8195 Å (see Figure 13). Lawson et al. (2009) construct an index based on the average flux off and on the doublet ($F_{8148-8172}/F_{8176-8200}$), whereas Schlieder et al. (2012a) use the EW summed over both lines. We measured both of these quantities for the Tuc–Hor candidates for which we obtained WiFeS spectra and list them in Table 5. The Na I index is measured in spectra that have been rebinned to a resolution of $R \sim 800$ to match that used in Lawson et al. (2009).

Figure 14 compares the Na I index with spectral type for Table 5 stars. Young low-mass candidates from the Rodriguez et al. (2011) study of TWA and Scorpius–Centaurus regions are

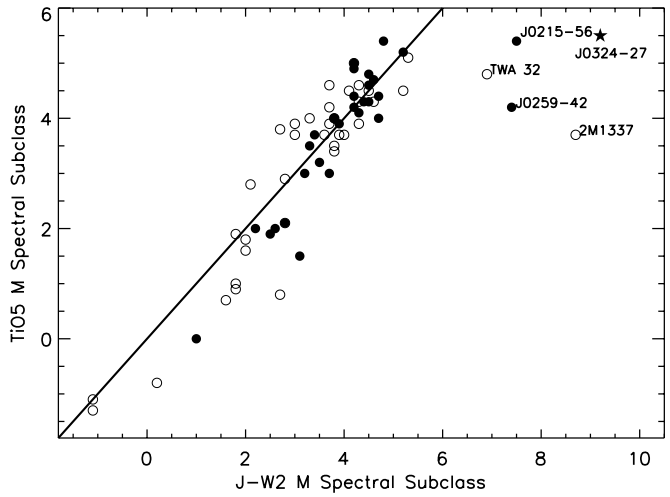

Figure 10. Comparison of M-dwarf spectral subtypes determined from $J-W2$ color (see Section 2.3) and the TiO5 index from optical spectra (Reid et al. 1995). Filled circles are from Table 2. Open circles are candidate young stars published by Rodriguez et al. (2011). J0324−27 is labeled with a star symbol to indicate that the spectral type is estimated from the near-IR spectrum (Section 3.3.2). J0259−42 and J0324−27 display clear signs of excess IR emission, while J0215−56 is more ambiguous (see Figure 18). The IR excesses around TWA 32 and 2M1337 have been previously noted (Schneider et al. 2012a, 2012b).

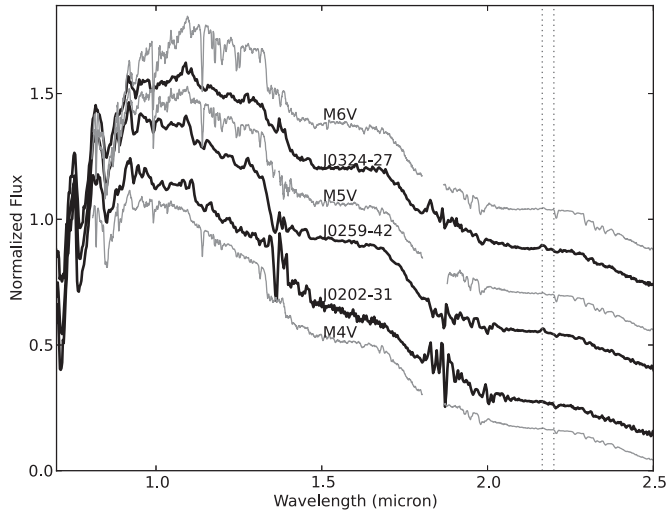

Figure 11. SpeX $R\sim100$ spectra for three of our Tuc–Hor candidates. Thin, gray spectra denote M6V, M5V, and M4V comparison field dwarfs from the IRTF SpeX Library. The vertical dotted lines indicate the location of the Br-γ and Na I features. J0259−42 and J0324−27 both show Br-γ emission and relatively weak Na I absorption. J0202−31 is a binary system.

also shown. Empirically determined trends for nearby ∼10 Myr old moving groups and (old) field dwarfs are also presented (Lawson et al. 2009), where we have used the relations in Kenyon & Hartmann (1995) to convert the Lawson et al. (2009) $R-I$ colors to spectral type. The Tuc–Hor candidates have higher Na I indices than the young (ages ∼ 10–20 Myr) candidates from Rodriguez et al. (2011), consistent with the older ages expected for Tuc–Hor members. While some Tuc–Hor candidates are close to the field dwarf line, these tend to lie in a region where the Na I index for young and old stars start to converge (i.e., spectral types earlier than about M4). The Na I 8200 Å doublet is therefore only useful as an age indicator for stars later than ∼M4, as also demonstrated by Schlieder et al. (2012a). Figure 14 indicates that most of the Tuc–Hor candidates lie in a region suggestive of an age older than ∼10 Myr, but younger than ∼1 Gyr.

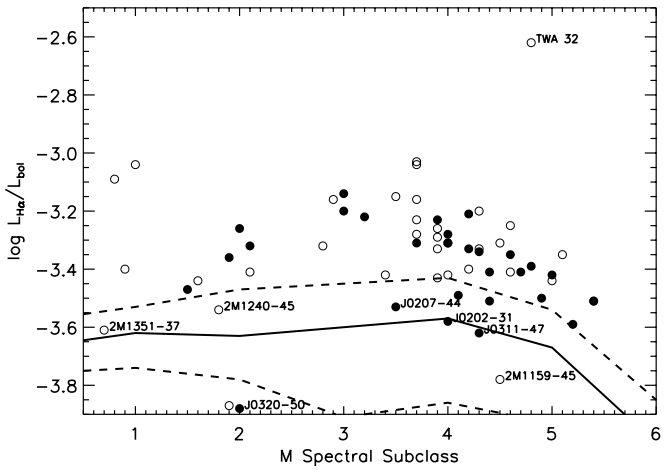

Figure 12. $L_{\rm H\alpha}/L_{\rm bol}$ for the Table 2 Tuc–Hor candidates for which we have measured Hα equivalent widths. The solid line indicates the average $L_{\rm H\alpha}/L_{\rm bol}$ for the field population studied in West et al. (2004) and its uncertainty (dashed lines) which includes the 1σ distribution of $L_{\rm H\alpha}/L_{\rm bol}$ (see Figure 5 in West et al. 2004). Solid circles are Table 5 stars. Open circles denote ∼10–20 Myr old TWA and Scorpius–Centaurus candidates from Rodriguez et al. (2011) analyzed in the same way. Some outliers in the figure are labeled.

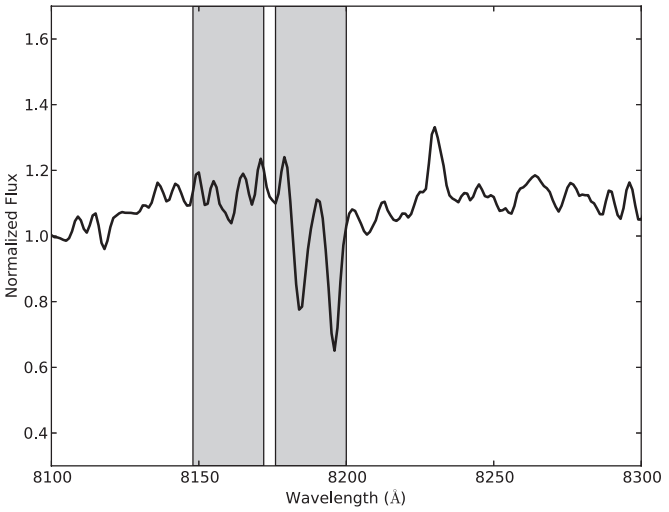

Figure 13. Spectrum for J0259−42, showing the region around the sodium doublet at 8183 and 8195 Å. Highlighted in gray are the two regions used to compute the Na I index (see Section 3.3.4 and Lawson et al. 2009).

3.4. X-Ray Emission

Of the 58 Tuc–Hor candidates, only 20 have X-ray detections in the ROSAT All-Sky Survey (RASS). Table 6 lists these *ROSAT* counterparts and their estimated values of $L_X/L_{\rm bol}$. To estimate the $L_X/L_{\rm bol}$ ratios, we convert the X-ray count rates to F_X (erg cm^{-2} s^{-1}) using an energy conversion factor (ECF) of 1.25×10^{11} (counts cm^2 erg^{-1}; Neuhaeuser et al. 1995) and bolometric fluxes calculated using the bolometric corrections listed in Kenyon & Hartmann (1995). The adopted ECF is similar to that used in prior studies for stars in the same general age range (i.e., 10–30 Myr; e.g., Kastner et al. 1997; Rodriguez et al. 2011 and references therein). For those stars without X-ray detection, we calculate an upper limit on $L_X/L_{\rm bol}$ by adopting a RASS flux limit of 2×10^{-13} erg cm^{-2} s^{-1} (Schmitt et al. 1995). All detections and most upper limits have log $L_X/L_{\rm bol}$ close to −3, the saturation limit for M-dwarfs (e.g., Riaz et al. 2006). The one notable exception is J0324−39, with log $L_X/L_{\rm bol}$ of −2.26. It is thus possible this star may have been observed by RASS

Table 6
ROSAT X-Ray Data for Table 2 Sources

Object	Dist. (pc)	log $L_{bol}/L_{\odot}$	X-Ray Counterpart 1RXS	Offset ($''$)	X-Ray Count Rate (s^{-1})	log L_X/L_{bol}
J0207−44	46	−1.17	J020701.9−440645	7	0.076 ± 0.014	−3.23
J0212−58	50	−1.09	J021257.7−585109	10	0.185 ± 0.053	−2.84
J0213−46	115	−0.44	J021329.9−465452	4	0.106 ± 0.017	−3.01
J0220−58	45	−1.53	J022052.8−582328	16	0.056 ± 0.020	−3.01
J0221−58	95	−1.03	J022145.6−583159	22	0.034 ± 0.016	−3.08
J0222−60	32	−1.36	J022243.9−602243	6	0.357 ± 0.042	−2.68
J0233−18	81	−1.00	J023400.1−181155	4	0.102 ± 0.020	−2.78
J0236−52	43	−0.86	J023651.8−520300	4	0.332 ± 0.028	−2.95
J0241−30	45	−1.92	J024127.5−304921	7	0.029 ± 0.010	−2.91
J0242−53E	44	−1.60	J024202.5−535908	17	0.036 ± 0.012	−3.17
J0242−53W	44	−1.87	J024202.5−535908	7	0.036 ± 0.012	−2.89
J0250−34	49	−1.60	J025100.3−340914	12	0.066 ± 0.016	−2.81
J0254−51	46	−0.90	J025432.4−510829	8	0.122 ± 0.022	−3.28
J0305−37	82	−0.76	J030510.1−372507	4	0.050 ± 0.015	−3.32
J0308−38	61	−1.74	J030840.1−384439	7	0.059 ± 0.014	−2.53
J0311−47	47	−1.62	J031145.2−471936	14	0.028 ± 0.010	−3.19
J0324−39	47	−1.40	J032439.7−390421	11	0.395 ± 0.039	−2.27
J0352−28	57	−1.19	J035222.3−282610	19	0.070 ± 0.014	−3.05
J0407−29	88	−0.48	J040710.6−291823	16	0.137 ± 0.019	−3.10
J0431−30	102	−0.82	J043137.9−304237	16	0.059 ± 0.018	−2.99
J0105−48	98	−1.66				<−2.56
J0127−60	48	−1.86				<−2.98
J0142−51	69	−1.53				<−2.99
J0150−58	48	−1.22				<−3.62
J0153−68	45	−1.91				<−3.00
J0154−29	58	−2.23				<−2.45
J0200−66	52	−1.65				<−3.13
J0202−31	55	−1.95				<−2.77
J0203−55	82	−1.47				<−2.91
J0205−60	44	−1.67				<−3.24
J0210−46	84	−1.47				<−2.88
J0215−56	50	−2.14				<−2.67
J0217−30	91	−1.13				<−3.16
J0217−32	101	−0.25				<−3.95
J0224−70	47	−1.57				<−3.28
J0232−57	51	−1.81				<−2.98
J0247−58	45	−1.19				<−3.71
J0250−65	56	−1.40				<−3.30
J0255−57	46	−1.96				<−2.92
J0259−42	106	−1.63				<−2.53
J0305−53	45	−1.97				<−2.92
J0310−36	45	−1.76				<−3.15
J0315−53	51	−1.90				<−2.90
J0316−35	43	−1.20				<−3.74
J0318−34	101	−1.13				<−3.07
J0320−50	50	−1.15				<−3.65
J0321−33	98	−1.30				<−2.93
J0324−27	114	−2.69				<−1.41
J0329−37	48	−1.69				<−3.15
J0336−26	50	−2.79				<−2.01
J0339−24	60	−2.52				<−2.13
J0341−22	77	−0.93				<−3.49
J0351−51	53	−1.60				<−3.16
J0356−39	56	−1.53				<−3.19
J0405−40	52	−1.29				<−3.48
J0413−44	64	−1.49				<−3.11
J0427−24	63	−2.62				<−1.99
J0427−33	72	−1.58				<−2.92

Notes. *ROSAT* X-ray counterparts to Table 2 sources along with estimated L_X/L_{bol}. For objects without X-ray detection, we adopt the ROSAT All-Sky Survey limit of 2×10^{-13} erg cm^{-2} s^{-1} provided in Schmitt et al. (1995). Distances listed are the Tuc–Hor kinematic estimates, but note that L_X/L_{bol} is independent of distance. Note that J0242−53E and J0242−53W match the same X-ray source.

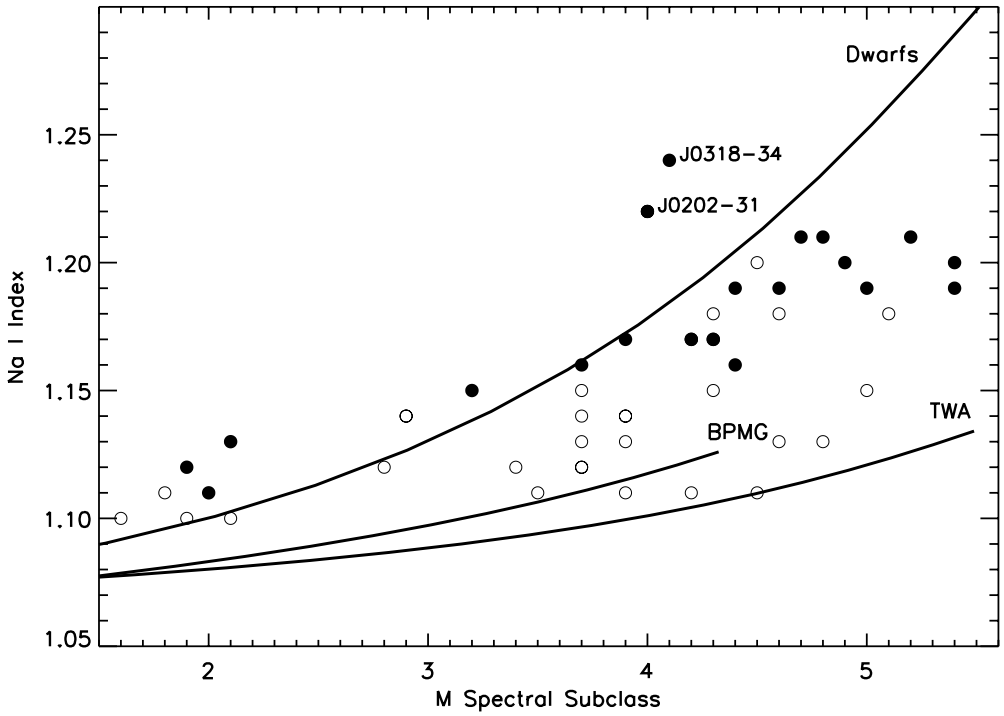

Figure 14. Na I index values (see Lawson et al. 2009 and Section 3.3.4) for the Table 2 Tuc–Hor candidates for which we have measured Na I (filled circles). The Na I index curve for TWA beyond M4.5 is not well constrained as only a single TWA member is used there (see Figure 1 in Lawson et al. 2009). Open circles denote ∼10–20 Myr old TWA and Scorpius–Centaurus candidates from Rodriguez et al. (2011) analyzed in the same way. For spectral types earlier than M4, the Na I index is not a reliable means to distinguish between older field dwarfs and young (>10 Myr) moving group members. The Na I indices of most of the Tuc–Hor candidates later than M4 appear consistent with ages intermediate between that of TWA or the β Pic moving group (which have ages ∼10 Myr) and the field dwarf population ($\gtrsim$1 Gyr).

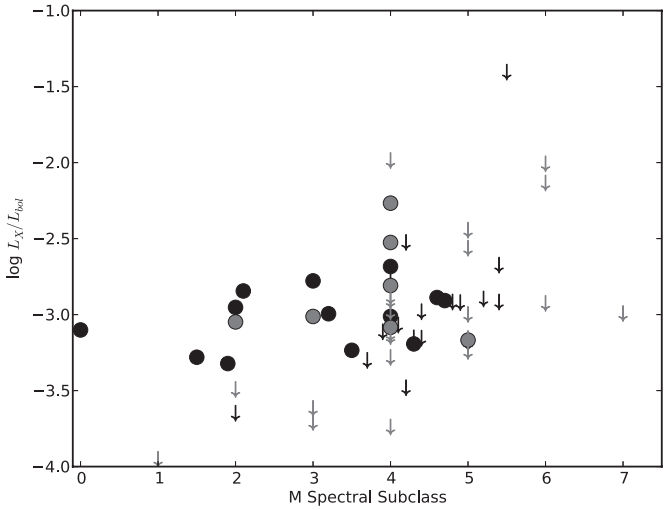

Figure 15. X-ray detections and limits for the Table 2 Tuc–Hor candidates. Dark gray symbols denote objects with spectral types estimated by their $J-W2$ colors. Downward arrows denote upper limits as described in Section 3.4.

Table 7
ROSAT X-Ray Detection Rates

Criteria	Number	Percent
This work	20/58	34^{+7}_{-6}
Rodriguez et al. (2011)	14/54	26^{+7}_{5}
<M4	10/17	58^{+10}_{-12}
⩾M4	10/41	24^{+8}_{-5}
Within 60 pc, <M4	6/11	54^{+13}_{-14}
Within 60 pc, ⩾M4	8/24	33^{+11}_{-8}

Notes. Distance are estimated from the convergent point method assuming Tuc–Hor membership. Stars with distances >60 pc may not be members of Tuc–Hor (see Section 3.5). Binomial errors are quoted for our percentages (Burgasser et al. 2003).

during a flare event. The X-ray detection fraction among our sample (20/58 = 0.34) is similar to that noted in Rodriguez et al. (2011) for TWA and Scorpius–Centaurus low-mass candidates (14/54 = 0.26).

Figure 15 compares L_X/L_{bol} versus spectral type for the Table 2 candidates; Table 7 summarizes the *ROSAT* X-ray detection statistics for the sample divided into bins of spectral type and distance. Figure 15 and Table 7 indicate that the frequency of RASS X-ray detections strongly depends on spectral type, i.e., the RASS detection frequency drops for stars M4 and later. The low rate of X-ray detections among our sample indicates that *GALEX* observations are capable of detecting active late M-dwarfs that have been missed in the RASS.

3.5. Comparison with BANYAN

Malo et al. (2013) published a Bayesian analysis tool (BANYAN) to estimate membership probabilities, distances, and radial velocities for candidates of known local young moving groups. The output is thus similar to that returned by the convergent point method employed here (Section 3.2) and serves as a useful comparison. In Table 4, we list the probabilities, distances, and radial velocities for the 58 Tuc–Hor candidates as estimated by both our convergent point analysis tool and that

Table 8
Comparisons of Distances for Known Tuc–Hor Members

Name	Parallax D (pc)	Conv. Point D (pc)	BANYAN D (pc)
HD 105	40.0	39.5	39.0
HD 987	44.0	47.9	47.5
HD 1466	41.0	44.0	43.5
HD 2884	43.0	45.5	44.5
HD 3003	47.0	46.4	45.5
HD 3221	46.0	46.4	45.0
HD 8558	49.0	46.9	45.0
CC Phe	37.0	41.3	40.5
DK Cet	42.0	41.7	40.5
HD 13183	50.0	51.2	47.5
HD 13246	45.0	46.6	44.5
phi Eri	47.0	47.9	45.0
epsilon Hyi	47.0	49.3	47.5
HD 22705	42.0	45.6	44.0
HD 29615	55.0	59.3	53.5
HD 30051	58.0	68.7	59.0
HD 32195	60.0	65.1	59.5
alpha Pav	56.0	56.4	57.0
HD 202917	46.0	48.9	50.0
HD 207575	45.0	48.2	48.5
HD 207964	47.0	48.4	48.5
DS Tuc	46.0	40.3	40.5

Note. Comparison of parallax distances (Torres et al. 2008) against convergent point kinematic distance and those distances predicted by BANYAN (Malo et al. 2013)

of Malo et al. (2013). The two tools return similar predicted radial velocities and kinematic distances, though the membership probabilities differ in detail. Comparing Tuc–Hor members with *Hipparcos* distances (Torres et al. 2008), we find good agreement between our kinematic distances, the BANYAN distances, and the *Hipparcos* distances (see Table 8). Given this agreement, we adopt a conservative uncertainty of ∼20% for our kinematic distances.

There are several cases where we find a high likelihood of Tuc–Hor membership with our convergent point analysis, but BANYAN returns a very low probability. In many of these cases, BANYAN returns a higher likelihood for membership in a different group. Furthermore, we find that for those objects with low BANYAN Tuc–Hor likelihoods, we predict much larger distances (∼60–120 pc) than the average Tuc–Hor member distances (most of which lie in the range 40–60 pc). Figure 16 shows the *XYZ* coordinates of the Table 2 candidates, adopting our kinematic distance estimates, and compares these *XYZ* values to those of known Tuc–Hor members from Torres et al. (2008). While most candidates have similar *XYZ* to those of known members, there are some prominent outliers (see the Appendix). For these outliers, BANYAN returns low likelihoods for membership in Tuc–Hor. Hence, the combination of probability and predicted distance in our convergent point analysis is analogous to the probability returned by the BANYAN code.

3.6. Notable Systems

Among Table 2 stars, there are several systems that are noteworthy for one or more reasons. For example, two systems (J0259−42 and J0324−27) have clear signs of an IR excess, as first noted in Section 3.3.2 (see also Figure 18), while another system, J0242−53EW, constitutes a wide separation low-mass

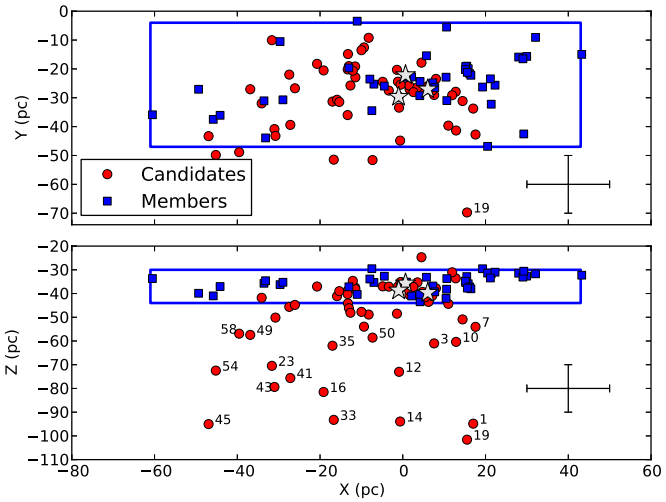

Figure 16. *XYZ* positions for candidates, adopting kinematic distances (see Section 3.2), compared to known members as drawn from Torres et al. (2008). *XYZ* is defined in the same fashion as *UVW*, with *X* positive toward the Galactic center, *Y* in the direction of Galactic rotation, and *Z* positive toward the north Galactic pole. The box outlines the spread of Tuc–Hor members (Torres et al. 2008). A 10 pc error bar is also shown, which corresponds to a 20% distance uncertainty at the typical distance of 50 pc. Prominent outliers are labeled with their Table 2 index and are discussed in the Appendix. The three star symbols represent the three candidate Tuc–Hor members listed in Table 9 and shown in Figure 17.

(A color version of this figure is available in the online journal.)

binary. Other systems have been previously mentioned in the literature; for some systems, we have measured radial velocities. For systems with radial velocities, we calculate *UVW* velocities and list them in Table 9. Some Table 2 stars appear to have low likelihoods ($\lesssim$60%) of Tuc–Hor membership using the convergent point analysis or the Bayesian methodology of Malo et al. (2013), but have higher likelihoods for membership in other groups. These noteworthy stars are discussed individually in the Appendix. Candidates that remain plausible members of moving groups (after the discussion in the Appendix) are summarized in Table 10, but we caution that measurements of radial velocities and distances will be necessary to fully confirm or rule out membership.

4. SUMMARY

We have carried out an all-sky *GALEX*–*WISE*–2MASS search for nearby ($D \lesssim 100$ pc), young (age 10–100 Myr), low-mass (mostly M-type) stars. We refer to this search as GALNYSS. On the basis of their UV/IR colors and space motions, where the latter are inferred from PMs and photometry, we identify 2031 candidate nearby, young M stars. The spectral type distribution of these candidates peaks near M3–M4. Most prior searches for young stars in nearby moving groups have focused on bright stars or on those with X-ray emission. Hence, these searches have tended to lack the sensitivity to detect the mid-M stars that dominate the list of nearby, young star candidates we have identified via GALNYSS. Given that M3–M5 stars constitute about half of all stars in the solar neighborhood, our survey thereby helps fill an important niche in the study of nearby young moving groups.

We consider a subset of 58 low-mass stars among the larger GALNYSS sample that lie in the vicinity of previously proposed members of the Tucana–Horologium association. We have developed and applied a grouping algorithm to select

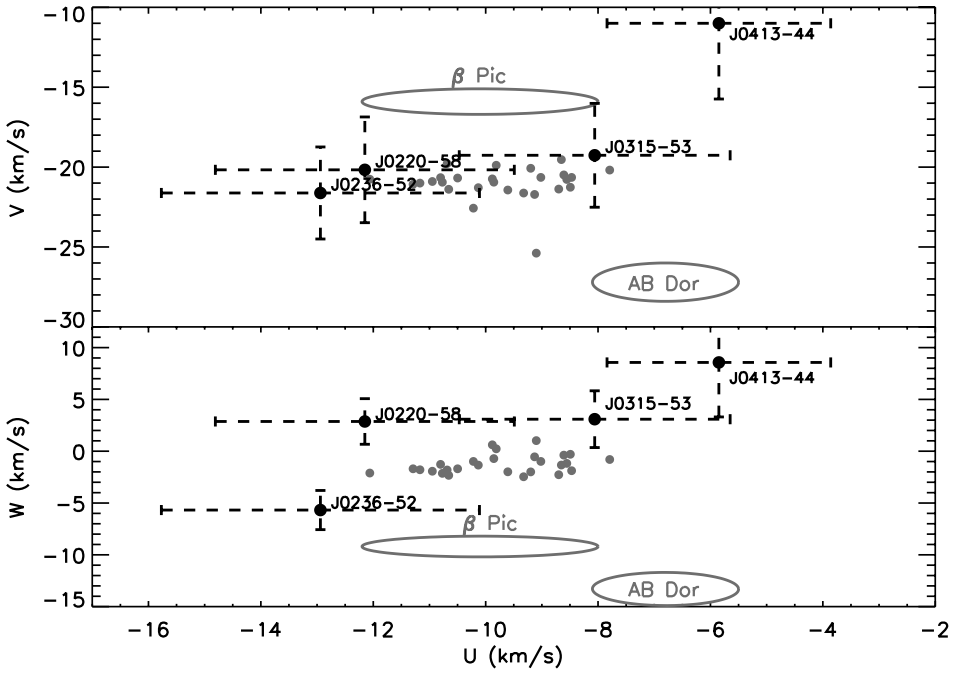

Figure 17. *UVW* velocities for candidates (see Table 9 and the Appendix) with measured radial velocities compared to several young moving groups (Torres et al. 2008). A distance of 42 pc is used for J0236−52. J0220−58, J0236−52, and J0315−53 have *XYZ* consistent with Tuc–Hor membership as shown in Figure 16. The small gray circles correspond to members of Tuc–Hor (Torres et al. 2006, 2008).

Table 9
UVW Velocities for Stars with Measured Radial Velocities (See the Appendix for More Details)

ID	D (pc)	RV (km s^{-1})	U (km s^{-1})	V (km s^{-1})	W (km s^{-1})
J0202−31	60[a]	16.7 ± 1.5	−14.2 ± 2.4	−24.2 ± 4.2	−9.3 ± 2.0
J0220−58	48	7.4 ± 1.5	−12.2 ± 2.7	−20.2 ± 3.3	2.9 ± 2.2
J0259−42	100[a]	15.3 ± 1.5	−10.7 ± 2.7	−21.8 ± 3.5	−3.7 ± 2.5
J0315−53	49	9.4 ± 1.5	−8.1 ± 2.4	−19.3 ± 3.3	3.1 ± 2.7
J0413−44	56	2.3 ± 6.6	−5.9 ± 2.0	−11.0 ± 4.7	8.6 ± 5.3
J0236−52	42	16 ± 1	−12.9 ± 2.8	−21.6 ± 2.9	−5.7 ± 1.9
	25[b]		−7.7 ± 1.9	−16.3 ± 2.0	−8.9 ± 1.4

Notes. Distances have uncertainties of 20%. The average *UVW* for Tuc–Hor members is −9.9 ± 1.5, −20.9 ± 0.8, −1.4 ± 0.9 km s^{-1} (Torres et al. 2008).
[a] Kinematic distance assuming membership in the Columba association. The average *UVW* velocity for Columba members is −13.2 ± 1.3, −21.8 ± 0.8, −5.9 ± 1.2 km s^{-1} (Torres et al. 2008).
[b] Isochrone distance from Torres et al. (2000) and Zuckerman & Song (2004).

these stars, and we further confirm them as a kinematically coherent group via convergent point and Bayesian analyses (Malo et al. 2013). Optical and near-IR spectroscopy obtained for some of the subsample of 58 Tuc–Hor candidates appear to confirm their young ages (∼30–100 Myr), based on their H emission lines and Li and Na I absorption line strengths. The color–magnitude diagram positions of the candidate Tuc–Hor members (as inferred from their kinematic distances) relative to those of low-mass IC2391 members also indicate that the candidates are likely younger than ∼50 Myr. Only roughly one-third of the sample objects are detected in the ROSAT All-Sky X-ray Survey, indicating that *GALEX* is capable of identifying young stars that are too faint to have been detected in the most sensitive extant all-sky X-ray survey.

We find that half of the 58 candidates have kinematic and spectroscopic properties consistent with membership in Tuc–Hor (Table 10). Many of the other candidates may instead be members of other young groups. Specifically, 2 stars are potential members of the AB Dor moving group, while 12 may be new Columba association members. Two of the Columba candidates have IR excesses indicating the presence of warm circumstellar disks in these systems. While the 15 remaining stars among the group of 58 do not have kinematics that might place them among the known young moving groups, their UV excesses suggest they nevertheless could be young; these stars warrant further examination.

Radial velocity measurements of these 58 candidate young, low-mass stars will be required to further confirm membership in Tuc–Hor or in other young moving groups. In subsequent work, we will explore the youth and kinematics of other subgroups among the list of nearby, young star candidates compiled for the GALNYSS.

We thank the anonymous referee for useful feedback that strengthened this paper. This publication makes use of data products from *GALEX*, operated for NASA by the California

Table 10
Candidate Summary Table

WISE	Group	*Ks*	$R - Ks$	Sp.	Conv. Point		BANYAN	
Designation		(mag)	(mag)	Type	Prob.	Dist.	Prob.	Dist.
J012758.87−603224.5	TH	10.2	4.4	M4.0	96	49	98	47
J015057.01−584403.4	TH	8.6	4.0	M2.9	95	48	97	46
J015325.09−683322.8	TH	10.2	4.9	M5.1	79	45	99	44
J020020.08−661402.0	TH	9.9	4.7	M4.3	79	52	98	50
J020701.85−440638.3	TH	8.4	3.4	M3.4	99	46	98	44
J021258.28−585118.3	TH	8.4	3.6	M2.1	95	50	96	47
J021533.37−562717.6	TH	11.0	5.3	M5.4	94	50	95	47
J022051.50−582341.3	TH	8.8	4.2	M3.0	78	45	96	44
J022244.32−602247.7	TH	8.1	4.5	M4.0	58	32	65	33
J022424.69−703321.2	TH	9.5	4.7	M4.3	98	47	100	46
J023219.44−574611.9	TH	10.2	5.4	M4.4	66	51	95	48
J024127.29−304915.1	TH	10.3	4.6	M4.7	70	45	59	43
J024202.14−535914.7	TH	10.0	4.7	M4.6	55	44	92	42
J024204.15−535900.0	TH	9.3	4.7	M4.7	88	44	96	43
J024746.49−580427.4	TH	8.4	3.9	M3.0	92	45	95	44
J025022.35−654555.2	TH	9.4	3.8	M3.7	85	56	97	52
J025059.67−340905.3	TH	9.6	4.2	M4.5	70	49	58	46
J025433.25−510831.4	TH	7.8	3.3	M1.5	100	46	97	44
J025531.87−570252.3	TH	10.2	4.8	M4.9	93	47	95	45
J030505.65−531718.4	TH	10.3	5.2	M5.4	77	45	93	44
J031049.48−361647.3	TH	9.8	4.8	M4.3	49	45	96	43
J031145.52−471950.2	TH	9.6	4.0	M4.3	52	47	92	44
J031523.72−534253.9	TH	10.4	5.4	M5.2	64	51	87	47
J032440.63−390422.8	TH	9.0	4.1	M4.2	89	47	94	44
J032916.57−370250.2	TH	9.8	5.0	M4.3	52	48	95	45
J035122.95−515458.1	TH	9.8	4.3	M4.2	98	53	93	49
J035616.31−391521.8	TH	9.6	5.0	M5.0	98	56	65	50
J040539.68−401410.5	TH	9.0	4.4	M4.2	87	52	69	48
J041336.14−441332.4	TH	9.9	4.1	M3.9	97	64	81	54
J014246.89−512646.9	Col	10.1	3.7	M6.5	89	72	73	66
J023359.89−181152.5	Col	9.2	3.8	M3.7	85	85	97	77
J025901.49−423220.4	Col	11.4	4.4	M4.2	91	106	69	92
J030509.79−372505.8	Col	8.7	3.8	M1.9	65	81	95	73
J030839.55−384436.3	Col	10.4	4.8	M4.2	100	60	72	56
J032144.76−330949.5	Col	10.4	3.9	M5.8	52	96	78	83
J032443.06−273323.1	Col	11.7	5.0	M5.5	81	112	64	95
J033901.64−243406.1	Col	10.0	4.8	M5.9	56	58	71	53
J040711.50−291834.3	Col	8.2	3.2	M0.0	78	81	93	72
J042726.28−245527.4	Col	10.8	4.2	M4.5	90	55	77	51
J042745.66−332742.6	Col	10.4	5.1	M4.8	86	63	88	57
J043138.61−304250.9	Col	9.3	3.5	M3.2	77	90	87	77
J020306.68−554542.1	ABD	10.4	4.5	M4.5	100	73	69	69
J021053.50−460351.4[a]	ABD	10.3	3.8	M4.2	...	...	...	...

Notes. Final table of candidates for Table 2 sources after eliminating likely field contaminants. Candidates are listed by moving group (TH=Tuc–Hor, Col=Columba, and ABD=AB Dor) and sorted by R.A. Distances and membership probabilities are listed for the particular group. Spectral types are estimated from the TiO5 index or $J - W2$ color. *R* magnitudes come from NOMAD whose data in turn are drawn from USNO-B1 and UCAC2; an error of 0.3 mag is assumed. In the Appendix, we discuss several of these candidate young systems in more detail, highlighting those that remain unconfirmed or doubtful members of the listed groups. Further work is needed to fully confirm these as members of these groups.

[a] J0210−46 is a low-mass companion to AB Dor member CD−46 644; see the Appendix.

Institute of Technology; the Two Micron All Sky Survey, which is a joint project of the University of Massachusetts and the Infrared Processing and Analysis Center/California Institute of Technology, funded by the National Aeronautics and Space Administration and the National Science Foundation; and the *Wide-field Infrared Survey Explorer*, which is a joint project of the University of California, Los Angeles, and the Jet Propulsion Laboratory/California Institute of Technology, funded by the National Aeronautics and Space Administration. This work has used the SIMBAD database, operated at CDS, Strasbourg, France. This research was supported in part by NASA Astrophysics Data Analysis Program grant NNX12AH37G to RIT and UCLA. D.R.R. acknowledges support from project BASAL PFB-06 of CONICYT, a Joint Committee ESO-Government of Chile grant, and FONDECYT grant No. 3130520.

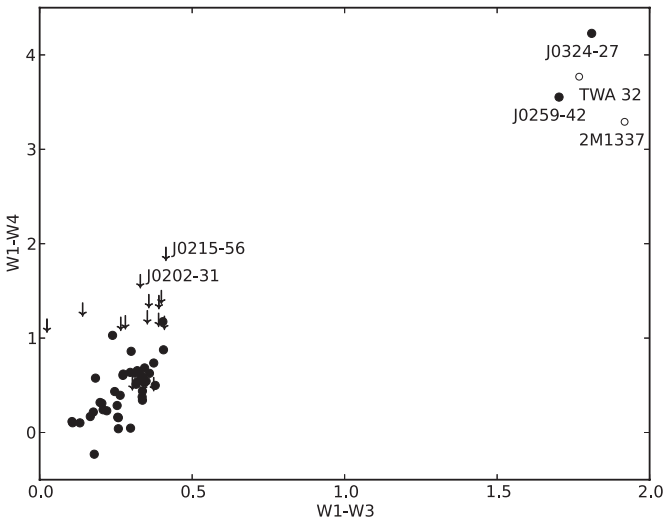

Figure 18. *WISE* $W1-W3$ and $W1-W4$ colors for the Table 2 Tuc–Hor candidates. Downward arrows denote systems for which only upper limits at $W4$ are available. J0259−42 and J0324−27 have clear infrared excesses, suggesting the possibility that warm ($T \sim 300$ K) dust orbits in a disk within these systems (see the Appendix). For comparison, the dusty systems in the sample of Rodriguez et al. (2011) are also shown and labeled (see also Schneider et al. 2012a, 2012b).

APPENDIX

NOTES ON INDIVIDUAL SYSTEMS

J0202−31. This M4 system has a higher likelihood of belonging to the Columba association (BANYAN: 74%, convergent point: 90%) than to Tuc–Hor (BANYAN: ∼20%, convergent point: 61%). While the kinematics favor Columba membership, the weak Hα emission and strong Na I absorption instead suggest the system may be old. With an $R \sim 7000$ WiFeS spectrum, we estimate a radial velocity of 16.7 ± 1.5 km s^{-1} and list calculated *UVW* velocities in Table 9. The *UVW* are a decent match to those listed in Torres et al. (2008) for Columba. Furthermore, the *XYZ* position (−10, −13, −58 pc) is also consistent with the *XYZ* of Columba members listed in Torres et al. (2008). Adopting an age 30 Myr (for Columba) yields reasonable agreement with the predicted kinematic distance (60 pc) assuming the object is an equal-components binary, as revealed by IRTF imaging (see Section 3.3.2). However, our spectroscopic observations of this system suggest an Hα luminosity consistent with that seen in old active stars (see Figure 12) and likewise Na I 8200 Å absorption that is stronger than expected for young stars (see Figure 14). The Na I doublet at 2.2 μm has EW of 4.8 Å, comparable in strength to that seen in a field M4 dwarf (∼4 Å). In comparison, other candidate Columba members of spectral type M5 have weaker Na I (J0259−42 and J0324−27: ∼3 Å) when compared to the field (M5: ∼7 Å). J0202−31, along with J0259−42 and J0324−27, has not been detected in X-rays, though this could be a combination of the spectral types (M4–5) and distances (60–100 pc) for these candidates. Hence, we conservatively infer that J0202−31 is not likely to be a member of Columba.

J0203−55. An M4.5 system with moderate BANYAN likelihood of membership in AB Dor (69%). Our convergent point analysis, however, predicts high likelihoods (99%) for either Tuc–Hor, Columba, or AB Dor. The radial velocity required for membership for these groups is 9, 13, and 25 km s^{-1}, respectively. However, the predicted distance for Tuc–Hor membership (∼80 pc) is large compared to that of known members. Our ∼100 Myr isochrone predicts a distance of 50 pc, which is moderately close to the kinematic distance as an AB Dor member (∼70 pc) given the 20% uncertainties. We tentatively list J0203−55 as an AB Dor candidate in Table 10, but caution that, as with most targets in this study, further work will be necessary to fully confirm membership.

J0210−46. This low-mass star forms a visual binary (21.″7 separation) with CD−46 644, a known AB Dor member (Torres et al. 2008). Although we removed young stars from Torres et al. (2008) as part of our analysis, this low-mass companion is not listed in their main AB Dor member table (see Table 13 in Torres et al. 2008, but see their Table 14) and was thus recovered here. Curiously, the UCAC4 PMs we have used yield higher likelihoods (>90%) of membership in Columba, in contrast to other PM estimates which place it in AB Dor. If bound, the CD−46 644 and J0210−46 system would have a separation of $a \sim 1500$ AU and binding energy of $-E = GM_1M_2/a \approx 15 \times 10^{41}$ erg, assuming masses of 0.85 and $0.15 M_{\odot}$. This is similar to the binding energies of known low-mass binaries; see the discussion of J0242−53EW below. Given the proximity to a previously proposed AB Dor member and possibility that it is bound, in addition to prior mention in the literature (Torres et al. 2008), we list J0210−46 as a plausible AB Dor member in Table 10.

J0220−58. This M3 system has a kinematic distance estimate of 48 pc and we measured a radial velocity of 7.4 ± 1.5 with WiFeS. The *UVW* velocities for J0220−58, listed in Table 9, match those of known Tuc–Hor members very well (see also Figure 17). While the $R \sim 7000$ WiFeS spectrum does not cover the Na I 8200 Å doublet, the Hα emission and lack of Li absorption is typical of other Tuc–Hor candidates and suggests a youthful age, but >10 Myr. The spectroscopic and kinematic properties suggest J0220−58 is a new low-mass member of Tuc–Hor.

J0236−52. This system, also designated as GSC 8056−0482, is an M2 star first considered a member of Tuc–Hor in Torres et al. (2000). However, both Torres et al. (2000) and Zuckerman & Song (2004) warn that its large lithium EW (∼300 Å) is inconsistent with Tuc–Hor membership. Such a large EW is indicative of a system younger than Tuc–Hor, a situation similar to that of J0315−53. We estimate a convergent point distance of 42 ± 8 pc, larger than previous photometric distance estimates of ∼25 pc (Torres et al. 2000; Zuckerman & Song 2004). These previous distance estimates are based on 30 Myr old isochrones, assuming the star is single. We note that Chauvin et al. (2010) rule out the presence of any close, low-mass companions on the basis of adaptive optics imaging. The discrepancy between the convergent point distance and the isochrone distance may be the result of uncertainties in the spectral type of the star, the isochrone models, or the convergent point estimate itself (although this seems unlikely, given the close agreement of convergent point distances with the parallax distances of known Tuc–Hor members; see Table 8). Another possibility is that the system is younger and hence more distant than expected, which would be more consistent with the measured lithium abundance. We note that our 10 Myr isochrone suggests a distance of 45 pc for this system, which implies J0236−52 should be closer to the Earth if its age were 30 Myr. While the BANYAN tool returns a 60% likelihood of Tuc–Hor membership, our convergent point analysis returns effectively 0%.

In Table 9 we list calculated *UVW* velocities using a previously measured radial velocity (16 ± 1 km s^{-1}; Torres et al. 2006) and distance estimates of 42 and 25 pc. In Figure 17 we plot the *UVW* velocities for this star for the 42 pc

distance estimate. While *UVW* velocities for the 42 pc distance (and also the 45 pc distance from our ∼10 Myr isochrone) are not a perfect match to those of Tuc–Hor, but they agree exactly with that of Columbia. The convergent point analysis and BANYAN tool return estimated distances of ∼40 pc, but with membership likelihoods of only 30%–40%. At a distance of 25 pc, the *UVW* velocities appear more consistent with the ∼10 Myr old β Pic moving group. While the Li absorption suggests a young age, comparable to that of β Pic, a parallax distance is essential if we are to place this system among the nearby moving groups. Given the conflicting results for this system, J0236−52 is not listed as a plausible Tuc–Hor or Columbia member in Table 10.

J0242−53EW. This system consists of a pair of M4.5 stars separated by ∼15″. We label the individual systems within the pair as the east (J0242−53E) or west (J0242−53W) component. Both show high likelihoods of membership in Tuc–Hor with a kinematic distance of 44 pc. At that distance, the pair of stars would be separated by ∼700 AU. A single X-ray source is detected with *ROSAT*. While we only have spectroscopy for J0242−53W, the spectrum are consistent with that of a >10 Myr dwarf. Membership in Tuc–Hor remains to be confirmed, but this represents a new wide-separation low-mass binary. Assuming a mass of ∼0.1 $M_{\odot}$ for each component, we estimate a binding energy of 2.5×10^{41} erg. While a minimum binding energy of $\sim 20 \times 10^{41}$ erg is typically cited for loose, low-mass binaries (Close et al. 2007, 2003; Burgasser et al. 2003), there is a growing population of systems with smaller binding energies comparable to or lower than that of J0242−53EW (e.g., see Figure 8 in Faherty et al. 2011).

J0254−51. This system, also designated as GSC 8057−0342, is an M1.5 star first identified by Torres et al. (2000) as a possible member of Tuc–Hor (referred to as the Horologium association in that paper). Lack of distance and radial velocity information prevented membership confirmation at the time. The reidentification of this candidate suggests future work is worthwhile to verify its membership status.

J0259−42. This system is one of only two candidates in our sample that display very red *WISE* colors (see Figure 18). Schneider et al. (2012b) note that $W1 - W4$ colors >1 among M-type systems are indicative of mid-IR excess and interpret this as the presence of a dusty circumstellar disk. The $W1 - W4$ color for J0259−42 is 3.6, an excess comparable to that seen in some TW Hya members such as TWA 31 and 32 (Schneider et al. 2012a). Only very young M-type stars show such mid-IR excess emission (Schneider et al. 2012b). On the other hand, lack of Li absorption suggests an age $\gtrsim$10 Myr. In terms of Na I absorption, J0259−42 is similar to the other Table 2 Tuc–Hor candidates, suggesting a similar age. Near-IR spectroscopy of J0259−42 (see Figure 11) reveals some signatures of youth, such as Br-γ emission and weaker Na I absorption than the field, but the distinctive triangular *H*-band profile seen in low-surface-gravity dwarfs is lacking. However, our kinematic distance estimate (108 pc) places it too far away for membership in Tuc–Hor. If J0259−42 were ∼10 Myr old, it would have a distance of ∼140 pc; in contrast, as an old field dwarf, it would lie only ∼40 pc away (Kraus & Hillenbrand 2007).

The radial velocity measured for J0259−42 with an $R \sim 7000$ WiFeS spectrum is 15.3 ± 1.5 km s^{-1}. The convergent point (Section 3.2) and Bayesian (Malo et al. 2013) methods both predict radial velocities of ∼17 km s^{-1} for membership in the Columba association, with kinematic distances of 106 and 92 pc, respectively. Our convergent point method yields a Columba membership likelihood of 92%, while BANYAN yields 69% (86% when including the radial velocity measurement). We calculate *UVW* velocities adopting a distance of ∼100 pc for this system assuming Columba membership (see Table 9). The *UVW* velocity uncertainties are high given the distance uncertainty of 20%, but the *UVW* are a good match to those listed in Torres et al. (2008) for Columba. Given that spectroscopic signatures point to a young age ($\gtrsim$10 Myr), J0259−42 may be a new member of the ∼30 Myr old Columba association, in agreement with kinematic indicators.

J0315−53. As mentioned in Section 3.3.3, this M5 system has strong Li absorption, indicative of a young age. However, the kinematics of the system agree with those of Tuc–Hor, which in turn appears inconsistent with the Li measurement. We have measured a radial velocity of 9.4 ± 1.5 km s^{-1} with an $R \sim 7000$ WiFeS spectrum. Table 9 lists calculated *UVW* velocities for the system assuming a kinematic distance of 49 pc. As Figure 17 illustrates, the *UVW* velocities match those of known Tuc–Hor members within the uncertainties. If J0315−53 were ∼10 Myr old, our empirical isochrones suggest a distance of 65 pc. However, the *UVW* velocities J0315−53 would have at that distance (-10.7 ± 3.2, -23.7 ± 4.3, 6.6 ± 3.5 km s^{-1}) do not match those of any known young groups. We note that this is not the first time a Li-rich low-mass star has been classified as a potential member of Tuc–Hor (see the discussion of J0236−52 above) and, hence, J0315−53 may indeed be a new Tuc–Hor member. A parallax distance measurement will be needed to fully confirm membership of this low-mass star.

J0324−27. Like J0259−42, J0324−27 also displays a strong IR excess (Figure 18); its $W1 - W4$ color is 4.2. The spectral type based on the $J - W2$ color (M9) is overestimated due to this excess, as is the case for J0259−42. Near-IR spectroscopy (Figure 10) suggests a spectral type intermediate between M5 and M6; we adopt M5.5. Furthermore, the SpeX spectra show some signatures of youth, such as Br-γ emission and weaker Na I absorption than the field, but, like J0259−42, J0324−27 lacks the low-surface-gravity *H*-band profile. Warm dust grains appear to be present in the system and also point toward a youthful nature. The kinematic distance estimate (∼110 pc) puts the star too far away for membership in Tuc–Hor. Columba membership, on the other hand, is likely: 60%–80% likelihood, with a distance of 90–110 pc. Overall, the system is very similar to J0259−42 and may be a young Columba member.

J0413−44. This M4 system was observed as part of the RAVE survey and has a published radial velocity of 2.3 ± 6.6 km s^{-1} (Siebert et al. 2011). A radial velocity closer to ∼16 km s^{-1} would be required for Tuc–Hor membership as seen in Table 4. The measured radial velocity, combined with our estimated kinematic distance (56 pc), allows us to estimate *UVW* velocities of -5.9 ± 2.0, -11.0 ± 4.7, and 8.6 ± 5.3 km s^{-1} (see Table 9). Hence, the *UVW* velocities for J0413−44 differ significantly from those of Tuc–Hor. With such a large, positive *W* velocity, it stands apart from many of the known young moving groups (see Figure 17). Indeed, given its measured radial velocity, we can find no distance for J0413−44 that would place it in the good *UVW* box. Therefore, while initially labeled as a Tuc–Hor candidate given its PMs, J0413−44 is not a member of Tuc–Hor and, furthermore, might not be a young star.

J0105−48, J0205−60, J0213−46, J0217−30, J0217−32. BANYAN predicts these systems lie among the field (old) population, rather than belonging to any particularly young moving group. Our convergent point analysis predicts a high likelihood of AB Dor membership (93%) for J0217−30 and

J0217−32, and a high likelihood of β Pic membership (87%) for J0213−46. However, the kinematic distances for these three stars (89, 97, 76 pc) are on the high end of what is typically observed for members of these groups and also differ when compared to the 10 and 100 Myr isochrone distances. Spectroscopy for these candidates will be necessary to search for features of youth and confirm whether or not they are old.

J0142−51, J0233−18, J0305−37, J0308−38, J0321−33, J0339−24, J0407−29, J0427−24, J0427−33, J0431−30. These systems are similar to J0202−31, J0259−42, and J0324−27 in the sense of high membership likelihoods (>60%) for the Columba association according to BANYAN. In many cases, the convergent point also returns a high likelihood of membership in Columba. Two systems, however, have low convergent point likelihoods of Columba membership (J0154−29: 21% and J0341−22: 45%). To be conservative, we do not list these two systems in Table 10. The other systems listed here remain viable candidates, but accurate radial velocities and distances will be necessary to fully vet their membership.

J0221−58, J0336−26. These two systems have equal BANYAN likelihoods (∼40%) for membership in two separate groups. J0221−58 may belong to either AB Dor or the old field population. The convergent point predicts a high probability of membership for AB Dor (∼95%). This M3.5 dwarf shows X-ray emission, but further work will be needed to ascertain the membership of the system. J0336−26, on the other hand, may belong to either Tuc–Hor or Columba, according to BANYAN. Our convergent point predicts equally high (∼70%) likelihood of membership in Tuc–Hor and Columba. A kinematic distance of ∼50 pc is predicted for either group, which is the same as what we estimate with the 10 Myr isochrone. Given the likelihoods of belonging to two separate groups, we refrain from placing either system in any young moving group until additional information is obtained.

J0316−35, J0320−50. These systems have very low convergent point likelihoods (<10%) of belonging to Tuc–Hor. However, BANYAN predicts moderate to high likelihood of membership (70%–90%). J0236−52, discussed above, is another such system where the convergent point analysis returns a low membership likelihood. Given the low convergent point likelihoods, we do not list them among plausible Tuc–Hor candidates in Table 10.

J0318−34, J0352−28. These objects have low likelihoods of Tuc–Hor membership, and higher for β Pic in both BANYAN and the convergent point methods. However, the 10 Myr isochrone distances for these stars (80, 100 pc) are much larger than the β Pic kinematic distances we estimate (50, 30 pc). Spectroscopy will be required to examine whether these stars are young enough to be β Pic members as implied by their kinematics. However, given the large distance discrepancies, we anticipate that these stars are unlikely to be new β Pic members.

REFERENCES

Allers, K. N., Jaffe, D. T., Luhman, K. L., et al. 2007, ApJ, 657, 511
Baraffe, I., Chabrier, G., Allard, F., & Hauschildt, P. H. 1998, A&A, 337, 403
Barrado y Navascués, D., Stauffer, J. R., Briceño, C., et al. 2001, ApJS, 134, 103
Bochanski, J. J., Hawley, S. L., Covey, K. R., et al. 2010, AJ, 139, 2679
Burgasser, A. J., Kirkpatrick, J. D., Reid, I. N., et al. 2003, ApJ, 586, 512
Burrows, A., Marley, M., Hubbard, W. B., et al. 1997, ApJ, 491, 856
Cardelli, J. A., Clayton, G. C., & Mathis, J. S. 1989, ApJ, 345, 245
Chauvin, G., Lagrange, A.-M., Bonavita, M., et al. 2010, A&A, 509, A52
Chauvin, G., Lagrange, A.-M., Dumas, C., et al. 2004, A&A, 425, L29
Chauvin, G., Lagrange, A.-M., Dumas, C., et al. 2005, A&A, 438, L25
Close, L. M., Siegler, N., Freed, M., & Biller, B. 2003, ApJ, 587, 407
Close, L. M., Zuckerman, B., Song, I., et al. 2007, ApJ, 660, 1492
Cushing, M. C., Vacca, W. D., & Rayner, J. T. 2004, PASP, 116, 362
Cutri, R. M., Skrutskie, M. F., van Dyk, S., et al. 2003, The IRSA 2MASS All-Sky Point Source Catalog, NASA/IPAC Infrared Science Archive, http://irsa.ipac.caltech.edu/applications/Gator/
de Bruijne, J. H. J. 1999, MNRAS, 306, 381
Dopita, M., Hart, J., McGregor, P., et al. 2007, Ap&SS, 310, 255
Dupuy, T. J., & Liu, M. C. 2012, ApJS, 201, 19
Faherty, J. K., Burgasser, A. J., Bochanski, J. J., et al. 2011, AJ, 141, 71
Faherty, J. K., Burgasser, A. J., Walter, F. M., et al. 2012, ApJ, 752, 56
Faherty, J. K., Rice, E. L., Cruz, K. L., Mamajek, E. E., & Núñez, A. 2013, AJ, 145, 2
Farihi, J., Becklin, E. E., & Zuckerman, B. 2005, ApJS, 161, 394
Findeisen, K., & Hillenbrand, L. 2010, AJ, 139, 1338
Findeisen, K., Hillenbrand, L., & Soderblom, D. 2011, AJ, 142, 23
Hambly, N. C., MacGillivray, H. T., Read, M. A., et al. 2001, MNRAS, 326, 1279
Hauschildt, P. H., Allard, F., & Baron, E. 1999, ApJ, 512, 377
Henry, T. J., Jao, W.-C., Subasavage, J. P., et al. 2006, AJ, 132, 2360
Hughes, A. M., Wilner, D. J., Kamp, I., & Hogerheijde, M. R. 2008, ApJ, 681, 626
Jones, D. H. P. 1971, MNRAS, 152, 231
Kastner, J. H., Zuckerman, B., Hily-Blant, P., & Forveille, T. 2008, A&A, 492, 469
Kastner, J. H., Zuckerman, B., Weintraub, D. A., & Forveille, T. 1997, Sci, 277, 67
Kenyon, S. J., & Hartmann, L. 1995, ApJS, 101, 117
Kirkpatrick, J. D., Cruz, K. L., Barman, T. S., et al. 2008, ApJ, 689, 1295
Kirkpatrick, J. D., Cushing, M. C., Gelino, C. R., et al. 2011, ApJS, 197, 19
Kraus, A. L., & Hillenbrand, L. A. 2007, AJ, 134, 2340
Lagrange, A.-M., Bonnefoy, M., Chauvin, G., et al. 2010, Sci, 329, 57
Lawson, W. A., Lyo, A.-R., & Bessell, M. S. 2009, MNRAS, 400, L29
Linsky, J., Redfield, S., Ayres, T., Brown, A., & Harper, G. 2001, in ASP Conf. Proc. 242, Eta Carinae and Other Mysterious Stars: The Hidden Opportunities of Emission Spectroscopy, ed. T. R. Gull, S. Johannson, & Kris Davidson (San Francisco, CA: ASP), 247
Looper, D. L., Bochanski, J. J., Burgasser, A. J., et al. 2010, AJ, 140, 1486
Lucas, P. W., Roche, P. F., Allard, F., & Hauschildt, P. H. 2001, MNRAS, 326, 695
Lyo, A.-R., Lawson, W. A., & Bessell, M. S. 2004, MNRAS, 355, 363
Malo, L., Doyon, R., Lafrenière, D., et al. 2013, ApJ, 762, 88
Mamajek, E. E. 2005, ApJ, 634, 1385
Marois, C., Macintosh, B., Barman, T., et al. 2008, Sci, 322, 1348
Marois, C., Zuckerman, B., Konopacky, Q. M., Macintosh, B., & Barman, T. 2010, Natur, 468, 1080
Martin, D. C., Fanson, J., Schiminovich, D., et al. 2005, ApJL, 619, L1
Mohanty, S., Basri, G., Jayawardhana, R., et al. 2004a, ApJ, 609, 854
Mohanty, S., Jayawardhana, R., & Basri, G. 2004b, ApJ, 609, 885
Monet, D. G., Levine, S. E., Canzian, B., et al. 2003, AJ, 125, 984
Neuhaeuser, R., Sterzik, M. F., Schmitt, J. H. M. M., Wichmann, R., & Krautter, J. 1995, A&A, 297, 391
Preibisch, T., & Feigelson, E. D. 2005, ApJS, 160, 390
Qi, C., Ho, P. T.P., Wilner, D. J., et al. 2004, ApJL, 616, L11
Qi, C., Wilner, D. J., Aikawa, Y., et al. 2008, ApJ, 681, 1396
Qi, C., Wilner, D. J., Calvet, N., et al. 2006, ApJL, 636, L157
Rayner, J. T., Toomey, D. W., Onaka, P. M., et al. 2003, PASP, 115, 362
Reid, I. N., Cruz, K. L., & Allen, P. R. 2007, AJ, 133, 2825
Reid, I. N., Hawley, S. L., & Gizis, J. E. 1995, AJ, 110, 1838
Riaz, B., Gizis, J. E., & Harvin, J. 2006, AJ, 132, 866
Rice, E. L., Faherty, J. K., & Cruz, K. L. 2010, ApJL, 715, L165
Riedel, A. R., Murphy, S. J., Henry, T. J., et al. 2011, AJ, 142, 104
Rodriguez, D. R., Bessell, M. S., Zuckerman, B., & Kastner, J. H. 2011, ApJ, 727, 62
Rodriguez, D. R., Kastner, J. H., Wilner, D., & Qi, C. 2010, ApJ, 720, 1684
Roeser, S., Demleitner, M., & Schilbach, E. 2010, AJ, 139, 2440
Schlieder, J. E., Lépine, S., Rice, E., et al. 2012a, AJ, 143, 114
Schlieder, J. E., Lépine, S., & Simon, M. 2012b, AJ, 143, 80
Schmitt, J. H. M. M., Fleming, T. A., & Giampapa, M. S. 1995, ApJ, 450, 392
Schneider, A., Melis, C., & Song, I. 2012a, ApJ, 754, 39
Schneider, A., Song, I., Melis, C., Zuckerman, B., & Bessell, M. 2012b, ApJ, 757, 163
Shkolnik, E. L., Anglada-Escudé, G., Liu, M. C., et al. 2012, ApJ, 758, 56
Shkolnik, E. L., Liu, M. C., Reid, I. N., Dupuy, T., & Weinberger, A. J. 2011, ApJ, 727, 6
Siebert, A., Williams, M. E. K., Siviero, A., et al. 2011, AJ, 141, 187

Siess, L., Dufour, E., & Forestini, M. 2000, A&A, 358, 593
Song, I., Bessell, M. S., & Zuckerman, B. 2002, ApJL, 581, L43
Stauffer, J., Tanner, A. M., Bryden, G., et al. 2010, PASP, 122, 885
Stauffer, J. R., Hartmann, L. W., Fazio, G. G., et al. 2007, ApJS, 172, 663
Stelzer, B., Marino, A., Micela, G., Lopez-Santiago, J., & Liefke, C. 2013, MNRAS, 431, 2063
Torres, C. A. O., da Silva, L., Quast, G. R., de la Reza, R., & Jilinski, E. 2000, AJ, 120, 1410
Torres, C. A. O., Quast, G. R., da Silva, L., et al. 2006, A&A, 460, 695
Torres, C. A. O., Quast, G. R., Melo, C. H. F., & Sterzik, M. F. 2008, in Handbook of Star Forming Regions, Vol. II: The Southern Sky, ed. B. Reipurth (ASP Monograph Publications Vol. 5; San Francisco, CA: ASP), 757
Vacca, W. D., Cushing, M. C., & Rayner, J. T. 2003, PASP, 115, 389
Walkowicz, L. M., Hawley, S. L., & West, A. A. 2004, PASP, 116, 1105
West, A. A., Hawley, S. L., Bochanski, J. J., et al. 2008, AJ, 135, 785
West, A. A., Hawley, S. L., Walkowicz, L. M., et al. 2004, AJ, 128, 426
White, R. J., & Basri, G. 2003, ApJ, 582, 1109
Wright, E. L., Eisenhardt, P. R. M., Mainzer, A. K., et al. 2010, AJ, 140, 1868
Yee, J. C., & Jensen, E. L. N. 2010, ApJ, 711, 303
Zacharias, N., Finch, C. T., Girard, T. M., et al. 2012, yCat, 1322, 0
Zuckerman, B., Bessell, M. S., Song, I., & Kim, S. 2006, ApJL, 649, L115
Zuckerman, B., Rhee, J. H., Song, I., & Bessell, M. S. 2011, ApJ, 732, 61
Zuckerman, B., & Song, I. 2004, ARA&A, 42, 685
Zuckerman, B., & Song, I. 2012, ApJ, 758, 77
Zuckerman, B., Song, I., & Webb, R. A. 2001, ApJ, 559, 388
Zuckerman, B., & Webb, R. A. 2000, ApJ, 535, 959